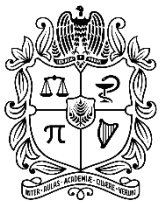

UNIVERSIDAD
NACIONAL
DE COLOMBIA

Blood flow computational characterization inside an idealized saccular aneurysm in presence of magnetic field.

Melisa Cardona Taborda

Universidad Nacional de Colombia

Facultad de Minas

Medellín, Colombia

2019

Blood flow computational characterization inside an idealized saccular aneurysm in presence of magnetic field.

Caracterización computacional del flujo de sangre en un aneurisma sacular idealizado en presencia de campos magnéticos

Melisa Cardona Taborda

Thesis for degree

in

Maestría en Ingeniería Mecánica

Director:

Juan Fernando Ramírez Patiño, PhD

Line of research

Biomechanics

Research Group

Grupo de Investigación en Biomecánica e Ingeniería de Rehabilitación (GIBIR)

Universidad Nacional de Colombia

Facultad de Minas

Medellin, Colombia

2019

To Professor Juan Fernando Ramírez P.,

Who always shares with me his never-failing enthusiasm that recharges my energy to never give up.

Acknowledgement

I would like to express my deep gratitude to Professor PhD. Juan Fernando Ramírez Patiño, my supervisor, and research tutor for his guidance and support throughout the course of all my research path. To Professor PhD. Aldo Germán Benavides Mora who have benefitted considerably my understanding of Computational Fluid Dynamics (CFD).
I would like to thank Professor PhD. Jean Paul Allain for challenging me with this thrilling topic. My grateful thanks are also extended to all the GIBIR research team, I am particularly grateful for the assistance given by Alejandro Rivera. I hope all the acquired knowledge can be transferred to his future living and working situations.

I am also grateful to the funding received through Fondos Sapiencia, from Alcaldía de Medellín, Colombia and Universidad Nacional de Colombia, Facultad de Minas Scholarships. A special thank you to Materialise colleagues and managers for being always committed to my personal and academic development, besides my engineer career growth.

Finally, I specially thank my parents and sister, for providing me with unfailing support throughout my years of study; and to Diego, for his continuous encouragement in all my goals and purposes. This accomplishment would not have been possible without them. Thank you.

Abstract

The blood flow of a wide neck saccular cerebral aneurysm is modeled using numerical methods, before and after positioning a diverter flow or stent as endovascular treatment. Blood, as a magnetic fluid, is modeled computationally under the influence of different external magnetic fields. For this, a list of factors that can be varied in the external magnetic field configuration and, in turn, can affect the velocity field of the blood flow of the stented aneurysm is selected. By varying the amplitude, direction and frequency of the magnetic field, it is concluded that the amplitude has an incidence on blood velocity and shear stress in the regions where the aneurysm starts and in the stent spires. After studying the changes in blood flow, a suspension of idealized endothelial cells is computationally injected, the trajectory is modeled and the cells that are trapped on the stent spires are quantified. With this, it is possible to understand the changes in the flow conditions of the cells and to examine whether, when the blood flow is subjected to an external magnetic field, it is possible to trap endothelial cells in the region of the stent. Trapped cells finally would promote complete occlusion of the neck of the aneurysm through the stimulation of tissue growth called endothelialization.

Keywords: Wide neck aneurysm, Endothelization, magnetic field fishing, Computational Fluid Dynamics, Magnetohydrodynamics.

Resumen

El flujo de sangre de un aneurisma cerebral, sacular de cuello amplio, es modelado usando métodos numéricos, antes y después de posicionar un diversor de flujo o stent como tratamiento endovascular. La sangre, como fluido magnético, es modelada computacionalmente bajo la influencia de diferentes campos magnéticos externos. Para esto, se selecciona una lista de factores que pueden ser variados en la configuración del campo magnético externo y a su vez pueden afectar el campo de velocidades del flujo de sangre del aneurisma con stent. Al variar la magnitud, dirección y frecuencia del campo magnético, se concluye que la magnitud tiene incidencia en la velocidad de la sangre y en el esfuerzo cortante en las regiones donde se inicia el aneurisma y en las espiras del stent. Después de estudiar los cambios en el flujo de sangre, se inyectan computacionalmente una suspensión de células endoteliales idealizadas, se modela su trayectoria y se cuantifican las células que son atrapadas por las espiras del stent en la región del cuello del aneurisma. Con esto, es posible comprender los cambios en las condiciones de flujo de las células y examinar si cuando el flujo de sangre es sometido a un campo magnético externo, es posible atrapar células endoteliales en la región del stent para finalmente promover la oclusión completa del cuello del aneurisma a través del estímulo del crecimiento de tejido llamado endotelización.

Palabras Clave: Aneurisma de cuello amplio, Endotelización, captura por campos magnéticos, Dinámica de fluidos computacional, Magneto-hidrodinámica.

Content

Figure List

Pág.

Table List

Pág.

Nomenclature and symbols

Symbol	Meaning	SI Units	Definition
Hypereslastic Model			
W	Strain Energy density		Eq.
I	Strain Invariants		
J	determinant of the gradient matrix of the deformation		Section
Herschel-Bulkley			
k	Consistency Index	$(kg \cdot s^{n-2}/m)$	
η	shear blood viscosity	$Pa \cdot s$	
$\dot{\gamma}$	Strain shear rate	s^{-1}	
τ_o	Yield Stress Threshold	Pa	
n	Power-law index.		
Carreau model			
$\mu_{\text{eff}}(\dot{\gamma})$			
μ_{inf}	Infinite Shear Viscosity		
μ_0	Zero Shear Viscosity for healthy blood	$^{\text{kg}}/_{\text{m s}}$	$22 \times 10^{-3}\ ^{\text{kg}}/_{\text{m s}}$
Ferro hydro dynamics model equations			
χ	Magnetic susceptibility.		
H	Applied magnetic field	T	
μ_o	magnetic permeability of vacuum	H/m	$4\pi\ \times 10^{-17} H/m$
μ	magnetic permeability		Eq.(4-7)
M	Magnetization		Eq. (4-4).
Magnetohydrodynamics model equation			Eq. (4-2) y
J	Current intensity		
c_p	Specific heat		

T	Temperature		ºC
σ	Electric conductivity		
B	magnetic flux density		
D	Diameter		
P	Pressure		
Q	Flow rate		
r	Radius		
V	Flow velocity		
μ	Dynamic viscosity		
ρ	Density		
Capture efficiency			
η	Capture efficiency		Eq. (3-1)
n_{in}	Number of particles arriving		
n_{out}	Number of particles leaving		
Discrete phase model			
F_{DPM}	Interparticle magnetic force		Eq. (4-12).
V_p	Particle velocity	m/s	
V_f	Carrier fluid velocity	m/s	
Particle Trajectories			
m_p	Particle mass	Kg	
F_s	Drag Force	N	Eq. (4-14)
F_m	Magnetization force	N	Eq. (4-15).
F_b	Buoyancy	N	
F_g	Gravity	N	
D_p	Particle diameter	M	
μ	Viscosity of the carrier fluid		
v_P	volume of the particle	m^3	
V_m	Magnetic velocity	m/s	
σ	electrical conductivity	S/m	

Acronyms:

Acronyms	Meaning
2/3D	Two-/three-dimensional
ACoA	Anterior communication artery
BCs	Boundary Conditions
BFD	Biomagnetic fluid dynamics
CAD	Computer-aided design
CFD	Computational fluid dynamics
DPM	Discrete phase model
DOE	Design of experiments
DSA	Digital Subtraction Angiography
EC	Endothelial cells
EPCs	Endothelial Progenitor Cells
FD	Flow Diverters
FDA	Food and drug administration
FHD	Ferrohydrodynamics
FSI	Fluid Stucture interaction
FVM	Finite Volume Method
HUVEC	Human umbilical vein endothelial cells
IA	Intracranial aneurysm
ICA	Internal carotid artery
MCA	Middle cerebral artery
MDT	Magnetic drug targeting
MHD	Magnetohydrodynamics
MNP	Magnetic nanoparticle
MRI	Magnetic resonance image
MRT	Magnetic resonance targeting
MSCs	Mesenchymal stem/stromal cells
NP	Nanoparticle
OSI	Oscillatory shear index
PCA	Posterior cerebral artery
PRT	Particle residence time

Acronyms	Meaning
Re	Reynolds Number
RMS	Root-Mean-Square
SAC	Stent assisted coil embolization
SI	International System of Units
UDF	User defined function
VSMCs	Vascular smooth muscle cells
WSS	Wall shear stress

Introduction

According to Brain Aneurysm Foundation, [1] almost 500,000 deaths worldwide each year are caused by brain aneurysms and half the victims are younger than 50. Several reports indicate that the clinical outcome of a ruptured aneurysm is extreme, over 8 – 10 per 100,000 people. 50% of the survivors have mortality of thirty-days, 25% of the patients suffer severe disability and the rest are at great risk for stroke, recurrent bleeding and other complications [1]–[3].

Current aneurysm treatments include physical occlusion via microsurgery or endovascular treatments. From the different kinds of aneurysm, wide-neck saccular aneurysms, tend to have an unfavorable anatomical configuration, leading to different concerns when deciding the best treatment [4]–[7].

The focus of aneurysms endovascular treatments has been to obtrude the blood flow to the aneurysmal sac. Recently, few ideas have emerged suggesting systems and methods that allow saccular aneurysm neck occlusion via re-endothelization of the missing tissue [8]–[10]. Options include to place a structural support that attract endothelial cells (EC) to induce tissue growth on the neck of the aneurysm, relieving fluid flow and pressure in the dome and significantly reducing or eliminating the possibility of a later rupture of the damaged vessel. This cell therapy represents a cutting edge approach with good forecast [11]–[13].

However, by the date, there are few strategies for localizing and deliver cells to target sites [14]–[16]. It includes the use of magnetic field to alter the cells trajectory. Nonetheless, there had been insufficient information about the effects on the adhesive properties of EC related with the long-term exposure on the disturbed flow, [2], [17]–[19].

Considering the cell magnetic attraction, to date, little is known about how EC respond to spatial variations in fluid shear stress at sites of aneurysm formation [10], [20], [21]

consequently, it is necessary to understand the behavior of the cells in the blood flow inside the stented aneurysm in presence of the magnetic forces, bearing in mind that there is still much to be learned from idealized computational models in the field of biofluid mechanics, where elemental flow description is still under construction [22]. In this thesis, the successful embolization of the aneurysm is computationally studied by characterizing the hemodynamic modifications caused by external magnetic field in combination with endovascular treatments.

- **AIMS**

This work aimed to describe the changes in the endothelial cells flow conditions in an idealized saccular brain aneurysm model, when a uniform magnetic field is applied as part of a novel treatment to recruit cells to the stent location

- **Specific Objectives**

1. To propose the representative geometrical configuration, the boundary conditions and the mechanical properties needed for calculating the disturbed blood flow parameters inside a wide-neck aneurysm in the presence of a uniform magnetic field.

2. To appraise the magnetic field amplitude, frequency, duration and direction required to attract and maintain endothelial cells to a specific region in the vessel, corresponding to an idealized saccular aneurysm neck.

3. To classify the factors incidence over the magnetic cells targeting efficacy.

4. To define mesh-independent solutions to achieve an appropriate grid for predicting the behavior of biomagnetic fluid flow in the presence of the magnetic field

.

- **SCOPE**

To calculate the blood flow pattern inside an idealized intracranial aneurysm under the presence of a uniform magnetic field using a computational analysis.

1. Theoretical Framework

This chapter presents a review of the experience gained in magnetically charged cells and particle delivery as a treatment for healing of endothelium in injured arteries. The first part of the chapter presents the theoretical framework related with brain aneurysm and their current treatments. Second part explores the strategies to occlude wide neck saccular aneurysm using cell therapy. Third part deals with researches on magnetic targeting, as a novel proposal that enable endothelial cell capture. It is described the physical model and the governing equations, based on the current knowledge gained from magnetic drug targeting (MDT).

1.1 Brain Aneurysm

Brain Aneurysm or Intracranial Aneurysm (IA) are pathological localized dilatations resulting from weakness in the cerebrovascular wall in direct communication with the lumen and blood flow [2], [23], [24]. IA can be classified according to their etiology, morphology, size and their location. Morphologically, IA can be classified as saccular, fusiform and dissecting aneurysms, where saccular aneurysms are the most common. Saccular aneurysms have a neck, which connects the aneurysm to the main blood vessel and a larger rounded portion called the dome, as presented in Figure 1-1. Neck and dome features help also to classify saccular aneurysms. They can be small, when the dome is around D=10 mm in diameter, large (H) with dome diameter range between 10–25 mm, and giant, with a dome diameter more than 25 mm. Further, regarding the neck size (N), aneurysm could be named as wide-neck aneurysms, when the neck diameter is greater than N=4 mm, or the dome-to-neck ratio is less than N/D=2mm [2], [25].

Figure 1-1. Saccular brain aneurysm morphology

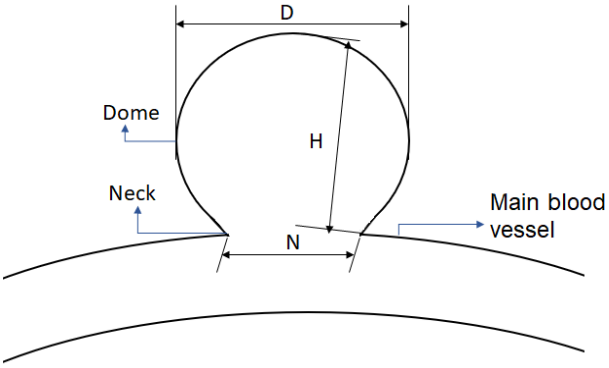

Figure 1-2, presents the most common sites of saccular aneurysms in the Circle of Willis. According with different studies, the order of prevalence of saccular aneurysm sites include anterior communicating artery (ACoA) (30%), junction of the internal carotid artery (ICA) and the posterior communicating artery (25%), the middle cerebral artery (MCA) bifurcation (20%) and at the ICA bifurcation (7.5%) [2], [26]–[29]. It is recognized that wide neck saccular aneurysms of the ACoA are considered the most complex of the anterior circulation, not only because of the diversity of the geometry but also for the complexity of flow conditions [30], [31].

Figure 1-2. Most common saccular aneurysm sites in Circle of Willis [28]

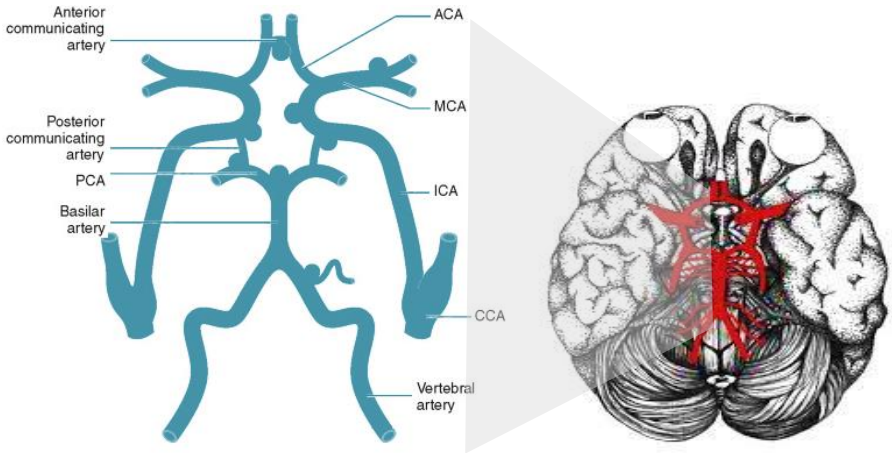

Besides the location, aneurysm rates of rupture are associated with morphologic factors. Considering the most common site for saccular brain aneurysm, multiple studies agree that size ratio, direction of the dome, and fenestration have mayor association with ACoA aneurysm rupture [29]

1.2 Brain Aneurysm Treatments

Currently, there are two main mechanisms to prevent bleeding or rebleeding of IA: Endovascular treatment and surgery. Minimally invasive endovascular management are mainly used for aneurysms of the basilar artery, and microsurgery is primarily used for peripheral aneurysms [2], [32] [33].

Surgical clipping.

Microvascular neurosurgical clipping allows to occlude the aneurysm by placing a titanium clip across the neck. Since it requires an open craniotomy, it is often considered in younger patients. This surgery leaves the risks of wound infection, unintended injury to other vascular structures and damage to the functions of close areas in the brain. Usually, it has a low rate of reoccurrence and rebleed, though it has the highest procedural morbidity and mortality [34], [35].

- **Embolization coils**

The goal of this endovascular embolization treatment is to decrease the blood flow inside the aneurysm dome, resulting in the exclusion of the aneurysm from the cerebral circulation.

To date, embolic coiling is the most commonly used endovascular treatment, nevertheless, for wide-neck aneurysms is still a challenge and in many cases, ineffective [4], [7]. The coils themselves may be prone to unraveling and migration inside the parent artery of the aneurysm, which can require further intervention to perform corrective actions like reposition the coils or its removal.

- **Stent assisted coil embolization (SAC).**

It has become a great treatment for wide-necked intracranial aneurysms, since it minimizes the risk of coil herniation, shear stress on the untreated aneurysm wall and compromise to the parent vessel. In this treatment, a protective mesh is used around the

aneurysm neck, forming a scaffold upon the neck, where endothelial cells can grow until the occlusion. However, after the treatment, patients must use antiplatelet agents to prevent periprocedural thromboembolic complications, and it is still unknown whether the occlusion status of aneurysms is associated with delayed ischemic events [36], [37].

- **Liquid Embolic Agents**

With the same goal of coiling, this treatment looks for excluding the aneurysm from the circulation by injecting polymers into the aneurysm sac. Being a liquid, the polymers have the advantage of conforming the complex aneurysmal shapes and can fill completely the dome. This treatment is challenging for cerebrovascular aneurysms due to concerns regarding reflux, distal embolization from polymer fragments and perforator and parent vessel occlusion [35].

- **Flow diverter:**

This less invasive treatment option places a flow diverter across the neck of the aneurysm, redirecting blood to the parent vessel. It promotes the creation of thrombosis within the aneurysm neck, where the blood clot acts like a scar, contracting over time promoting an aneurysm shrink [38], [7], [36] [39]

This treatment is becoming popular for some of the complex proximal internal carotid artery aneurysms [38]. Nonetheless, the risks associated with the flow diverter treatment of unruptured aneurysms has not yet been fully quantified [22]. Since flow diverters work over time, there is a small risk of aneurysm rupture before the total occlusion, especially for wide neck aneurysms. The blood clot also triggers an inflammatory reaction, which can increase the risk of rupture in extremely large and fast-growing aneurysms and in those locations with very thin walls [39].

- **Drug-eluting stent (DES)**

This treatment is a remarkable development where the stent has the ability of providing controlled release of therapeutic agents to promote neck occlusion. However, the potent antiproliferative drugs released cause extensive endothelial denudation and inhibits endothelialization of the implanted stent struts, which is an important predisposing factor for thrombotic complications, in particular late stent thrombosis [40], [41].

There is a growing interest in finding a treatment that allows to promote complete occlusion of intracranial vascular lesions [42]–[44]. In this respect, regenerative medicine, specifically cell therapy, represents a cutting-edge approach with good forecast to contribute to durability of treatments.

Combining aforementioned treatments with cell therapies, it is easy to appreciate great potential for promoting complete occlusion of saccular aneurysm, by the ingrowth of the missing arterial wall across the stent scaffold. This proposal and the current progress in this field are discussed further in Chapter 2.

2. Aneurysm treatment via Reendothelization

Cerebral arteries consist of three layers: the intima, the media, and the adventitia. The intima is the innermost layer of the arterial wall and consist of a one cell thick sheet of endothelial cells (EC) also named endothelium. Endothelium is in direct contact with flowing blood and it has an important function in regulating the effects of hemodynamic forces on the functionality of the arterial wall.

Figure 2-1. Aneurysm layers [26]

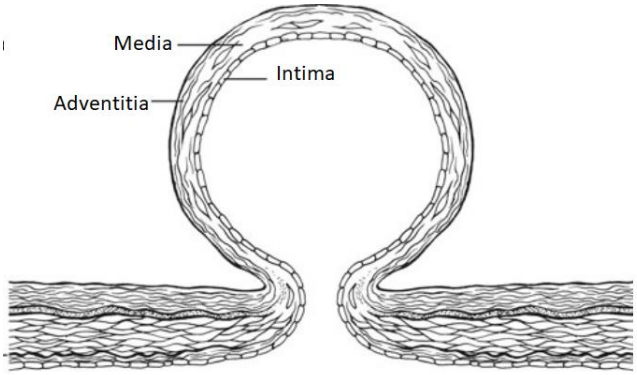

As presented in Figure 2-1, there is an abrupt termination of the tunica media at the edge of the aneurysm neck, leading to a bad integrity of the blood vessel. In this sense, the reconstruction of the tunica media across the orifice would promote durability of aneurysm occlusion [26], [41], [45]. To reconstruct the tunica media, it is required first to promotes endothelial proliferation in the neck, it means to promote the pseudo neoendothelization of the region [26].

Cell therapy using live cells to treat diseases is a rapidly growing area where reendothelization is studied to recuperate injured vessels [10], [22], [46], [47]. Different kind of cells have been reviewed in preclinical cell therapy studies for the treatment of

brain aneurysms like: Vascular smooth muscle cells (VSMCs), fibroblasts, Endothelial Progenitor Cells (EPCs), and Mesenchymal stem/stromal cells (MSCs), showing that EPCs have a great role in vascular tissue regeneration in general beside the feasibility of isolating [1], [38], [48].

It has been proposed to take advantage of reendothelization phenomenon to improve the current treatments for saccular brain aneurysm, where the regeneration of the missing tunica media in the saccular neck represents an ideal situation that avoid the blood to enter the sac and reduce the pressure that causes the rupture. Early thinking was coating stents with EC, but in addition to the clinical complications that it represents, none appear to have provided the safety and efficacy. [4], [22], [49].

It has been demonstrated that Flow Diverters reduce the blood flow inside the sac and depending on its porosity, it creates a scaffold upon which EPCs can merge themselves to create new tissue [27], [45], [50]–[52]. The new tissue formation is possible thanks to the conversion of mechanical stimuli into chemical activity called mechanotransduction, that can help to occlude the aneurysm neck. However, the time frame for complete occlusion is still unknown and the risk of rupture remains until the aneurysm is completely occluded [1], [3], [22]. Furthermore, the non-control of the tissue growth phenomenon or incomplete healing can lead to thrombogenic occlusion of the parent artery that likewise can lead to device failure and the need of clinical re-intervention [1]. To handle this issue, the vessel growth should be redirect and speeded up by increasing the EPCs attraction and maintenance rate to the stent thereby completing endothelialization only at the aneurysm neck [3], [4], [9].

Intrasaccular thrombosis and endothelial cell growth across the aneurysm neck have been observed after flow diversion in different *in vitro* and *in vivo* experiments [14], [44], [53] where it is suggested the existence of a relationship between the hemodynamic conditions created immediately after deployment of FD devices and the subsequent aneurysm occlusion. To better understand this healing process, the hemodynamics of the brain aneurysm should be studied.

2.1 Brain Aneurysm Hemodynamics

Hemodynamics is the dynamics of blood flow. It includes magnitude, direction and possible clinical role of the forces, moments and pressures acting on the blood artery. Regarding aneurysms, it has been demonstrated that the shape of the dome and the neck, and the properties of the afferent and efferent vessels alter the blood flows inside the aneurysm, making the intra-aneurysmal flow an unique pattern [27].

Recent studies are focusing the attention to the effect of blood flow in the pathogenesis and treatment of cerebral aneurysm. However, to date, no single hemodynamic parameter has been identified as the major factor responsible for aneurysmal formation nor its occlusion [27], [54], [55]. As presented in Figure 2-2, flow patterns differ in sidewall and bifurcation aneurysms. Hence, characterizing the hemodynamic parameters associated with this vascular malformation is still very important to understand the pathology and to propose improvements in its treatment.

Figure 2-2. Direction of flow inside a sidewall type aneurysm [27].

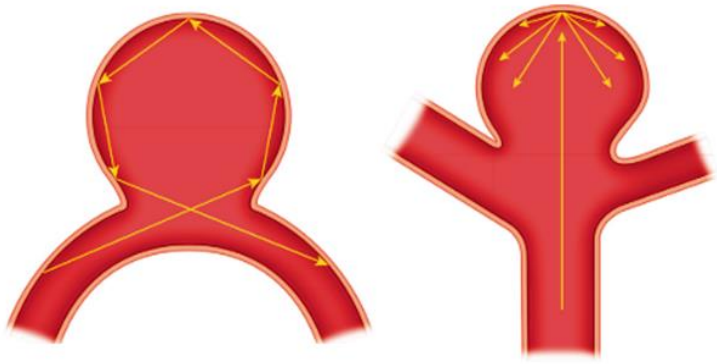

Aneurysm flow is usually studied at three main points: the distal aspect of the neck, the proximal neck and the entrance to the aneurysm, where the inflow entering the aneurysm, the outflow exiting the aneurysm and the central slow flow vortexes are characterized [54]. For the aneurysm hemodynamics studies, numerical simulations are common used those can be more or less accurate to biological reality depending on which formulas and assumptions are implemented. For instance, pulsatile or continuous flow conditions, Newtonian or non-Newtonian fluid considerations, rigid or elastic conditions on the vessel

wall, and patient-specific flow conditions or flow conditions from healthy individuals are relevant in the aneurysm hemodynamics results [27].

The most common variables studied for aneurysm treatments are: the changes in the velocity field, the vessel wall tension, flow stagnation and Wall shear stress (WSS) as the most well-studied force acting on vessel walls.

2.2 Wall shear stress and endothelial cell response

Wall shear stress (WSS), is the mechanical stress resulting from the tangential force exerted on the arterial wall by the blood flow. This dynamic frictional force is tangential to the wall and increases when the velocity or viscosity of the blood increases [27], [56].

WSS is the dominant force affecting EC behavior that contributes to good vascular health [46]. Despite the fact the influence of WSS in the endothelial cell response is not completely understood, it is hypothesized that the temporal and spatial variations in WSS is correlated with the growth and rupture of aneurysms [57], [58].

It is known that WSS stimulates the functions of EC, affecting the structural integrity of the endothelium, the transport of various cells and enzymes in the blood stream to the endothelium, and abnormal levels can cause dysfunction [22], [59]. In addition, it has been reported that high level of WSS induces vasodilators activation, promoting widening of the vessels, while low WSS, activates vasoconstrictors promoting vessels narrowing [22].

Ostrowski *et al,* [20] experimentally studied the endothelial cells migration and orientation under different controlled WSS. They found that ECs are exquisitely sensitive to both magnitude and spatial gradients in WSS. At high confluence, cells migrate against the direction of fluid flow and take place in the region of maximum WSS. In addition, the cells align parallel to the flow at low WSS.

A WSS of approximately 2 Pa is assumed to be suitable for maintaining the structure of the aneurysmal wall, while a WSS less than 1.5 Pa results in endothelial cells degeneration [58].

It is known that stent implantation changes the arterial blood flow patterns and consequently changes the magnitude and distribution of Wall Shear Stress (WSS), in particular FDs reduce WSS at the aneurysmal sac [54], [60]. Recently, Kutikhin *et al* [46] indicated that when laminar flow is applied, both high and low values of shear stress evoke beneficial effects in homing, and differentiation of EPCs *in vitro.*

3. Magnetically-labeled endothelial cells in Stented Vessels

Increasing the EPCs capture and maintenance rate from the circulating blood stream onto surfaces have gained importance during last years and different strategies for EPCs fishing have been proposed, such us surface modifications, antibodies, peptides, oligosaccharides, nucleic acid species and magnetic fields [19], [38], [61].

Comparisons among the different cell enrichment methodologies have presented several advantages of magnetic separation [62], [63]. It includes, high selectivity, specificity and tunability where the ability of controlling cells from distance makes feasible to attract cells over a wider spatial domain. Those advantages are presented both for fishing cells with inherit magnetic properties and cells labeled with magnetic nanoparticles.

In 1977, Magnet-activated cell sorting (MACS) was introduced by Molday *et al* [64] when extrinsic magnetic bead labeling was presented. Afterwards, Consigny *et al.* [65] used cell encapsulation to incorporate magnetic nanoparticles to manipulate cell by external magnetic fields. They presented the phagocytosis phenomenon with microspheres, to promote cell delivery and retention using magnetic targeting as an advanced cell therapy. However, it was found that the presence of superparamagnetic microspheres change the profile of the cells, decreasing cell retention after exposure to a fluid shear [8], [16]. Afterwards, with the nanotechnology development, the size of the particles was reduced allowing to load EC with Magnetic nanoparticles (MNPs) [66]. The use of MNPs under a high gradient magnetic field without adversely affecting the cell viability, function and proliferation capacity, made possible the use of magnetism to guide endothelial cell to stented arterial regions [11], [12], [67].

3.1 Magnetic Nanoparticles characterization

Currently around 20 different magnetic particles have been experimentally used for labeling cells, where Magnetite Fe_3O_4 and maghemite γ-Fe_2O_3 are by far the most commonly employed oxides. Its selection generally depends on cell uptake, toxicity and magnetic properties required [15].

Prior cell labeling, MNPs are encapsulated in a corona of hydrophilic macromolecules to avoid their uncontrolled aggregation and delay their clearance by the mononuclear phagocyte system. Once the particles are inside the cell, it has been demonstrated that particles are metabolized in lysosomes surrounding the cell nucleus. Finally the labeled cell gains enough magnetization to be detectable by MRI and/or to be manipulated by an external magnetic field. [68], [69].

From the MDT studies it is known that MNPs will be attracted towards the surface of magnets. When a magnetic field is applied to MNPs inside cells, it generates an intracellular force. Cells appear to prefer moving as an entirety rather than undergoing intracellular displacement, which is also a self-defense method to maintain the mechanical structure of the cell as a system [69].

Shen *et al* [70], studied how cells sense force and how mechanical signals are transferred inside the endothelial cells after functionalizing them with MNPs. Using approximately 23000 MNPs per cell, roughly 0.63 pg ferroferric oxide per cell, they demonstrated experimentally that the magnetic force promoted cell migration in certain directions. In the absence of a magnetic force, cells tend to migrate to a less crowded place while under the magnetic field, a small bump formed over the magnets location.

MNP have demonstrated biocompatibility, biodegradability, ease of synthesis and absence of hysteresis [50] and to date MNPs and Magnetic fields are being used different cell therapies like cells accumulation in stented vessels or directing cells to damaged tissues for tissue regeneration [48], [71].

Different experimental approaches have been proposed to achieve rapid and stable cell homing and expansion in stented arteries via magnetically guided delivery of EC functionalized with biodegradable MNPs.

In their review Sensenig *et al.* [72], presented the use of tissue engineered scaffolds in regenerative applications. Preload the cells with biodegradable polymeric superparamagnetic nanoparticles and using a uniform external magnetic field inducted the stent and the particles with magnetic field gradients. They showed that the cells are magnetized even sufficiently far away from the gradient source, because the MNP-loaded cells magnetic moments remain independent on the distance from this source.

Patent WO2013052934 proposed by J.P Allain *et al* [11], describes that the stent seeded with endothelial cells, can be coated using magnetic bacterial nanocellulose (MBNC), a unique biopolymer, which can be used as a scaffold for initial magnetically-labeled endothelial cell attraction and attachment.

According with Tibbe *et al* [73] for labeled cells separation, the time depends not only on the size of the field gradients but also on the size, shape, density of cells, number of immunomagnetic particles per cell, size of these particles, and height of the chamber

Uthamaraj *et al*. [74], proposed to magnetize stents to attract and retain magnetically-labeled endothelial cells delivered post implantation. They delivered cells directly to the magnetic stent and occluded the blood flow for a short period (2 min). Then with the first monolayer of EC, a rapidly capturing of cells occurs once restoring the blood flow conditions. In this proposal magnetic-labeled cells are attracted to all parts of the scaffold, being a not applicable method for occluding localized regions like aneurysmal neck.

Arias *et al* [50], identified that nanobacterial cellulose (NBC) can act as a frame where cells can be attached, grow, proliferate and conclusively begin to close the aneurysm neck *in vivo.* She proposed, via a chemical thermal process, to create a magnetic nanobacterial cellulose to recruit cells to the specific stent location.

In tissue engineering studies, scaffolds are 3D structures where seeding cells can be attached and enhance their proliferation and differentiation, in this sense stents have an

inherent thrombogenicity [9]. In addition, due to their chemical composition, commercially available stainless steel stents has a paramagnetic nature that have been used for targeting nanoparticle loaded endothelial cells to the entire stent surface in isolated blood vessels using external magnetic field [16], [49]. However, the technique should promote growth factor even after restoring blood flow. In this sense, a coat of a EC monolayer on the stent surface can accelerate the complete healing [11], [74].

After understanding the features required both for the magnetic-labeled cells and the scaffold to promote growth factors, the targeting efficacy across the stent scaffold under blood flow conditions is presented in the following session. In this sense, the magnetophoresis phenomenon that controls the migration of particles upon the application of a magnetic field is studied.

3.2 Magnetic cell targeting efficacy under flow conditions

It is well known that the prediction of capturing nanoparticles using magnetic field in the presence of the fluid shear *in vivo* is critical and different properties of the particles should be considered for the analysis of the magnetic targeting efficacy under flow conditions. For example, superparamagnetic properties are desirable since the particle can exhibit a large ferromagnetic response in the presence of a magnetic field but have zero response in the absence of a field. In addition, it will bring the ability of being ‘turned on and off’ when required [8], [62].

Shen *et al.* [75] showed in an *in vivo* comparison that the magnetic targeting effectiveness is not always related with the highest magnetic field strength, since it only occurs when the magnetism is applied in a short time frame, and taking into account the experience of drug vascular stents in the interventional therapy, a fully integration of tunica intima requires least 3 months [26], [76]. Associated to this, and taking into account the different results from MDT computational studies, it has been demonstrated that speeding up the capturing cells depends on several variables, such as: the interaction between magnetic strength, time of exposure, particle injection, flow conditions and particle features [25], [41], [77]–[80].

The minimum magnetic field reported to attract ECs is 0,3 T [75]. For the magnetic targeting efficacy study, the maximum strength of the magnetic field must be defined in terms of the non-harmful magnetic field in the human body accepted by Food and drug administration (FDA), reported to be 8T [81] and the magnetic field source, where either external, implanted magnets, permanent and electromagnet magnets have been studied [15], [62].

Electromagnets require a current source that allows to adjust the resultant magnetic field and can control the switched on/off. In contrast, permanent magnets have a fixed location and a change of the position leads to a different direction of the magnetic separation course. Magnetic resonance targeting (MRT), has been proposed as an option for magnetic cell delivery. In this method, magnetic field gradients, inherent to all magnetic resonance imaging (MRI) systems, are used to steer ferromagnetic particles to a target region [15]. There is different magnetic resonance (MR) scanners, that implies a different magnetic field direction to the aneurysm neck. Cylindrical scanners have a magnetic field along the symmetry axis of the cylinder, it means parallel to caudo-cranial direction, meanwhile an open bore MR magnetic field is perpendicular to head feet [82], [83]. Differences in the magnetic field direction can be appreciated in Figure 3-1, where magnetic flow lines are presented related with the horizontal position of a person. In addition, depending on the magnetic field amplitude, there is a frequency related with the machine following Larmor equation [84]. In addition to Electromagnetic MRI machines, there are also permanent MRI magnets that operate at field strengths typically ranging from 0.2T to 1.0T. These MRI use permanently magnetized iron where the two poles are close together and parallel, since the iron is twisted as a C shape [82].

Figure 3-1. MR scanner configurations

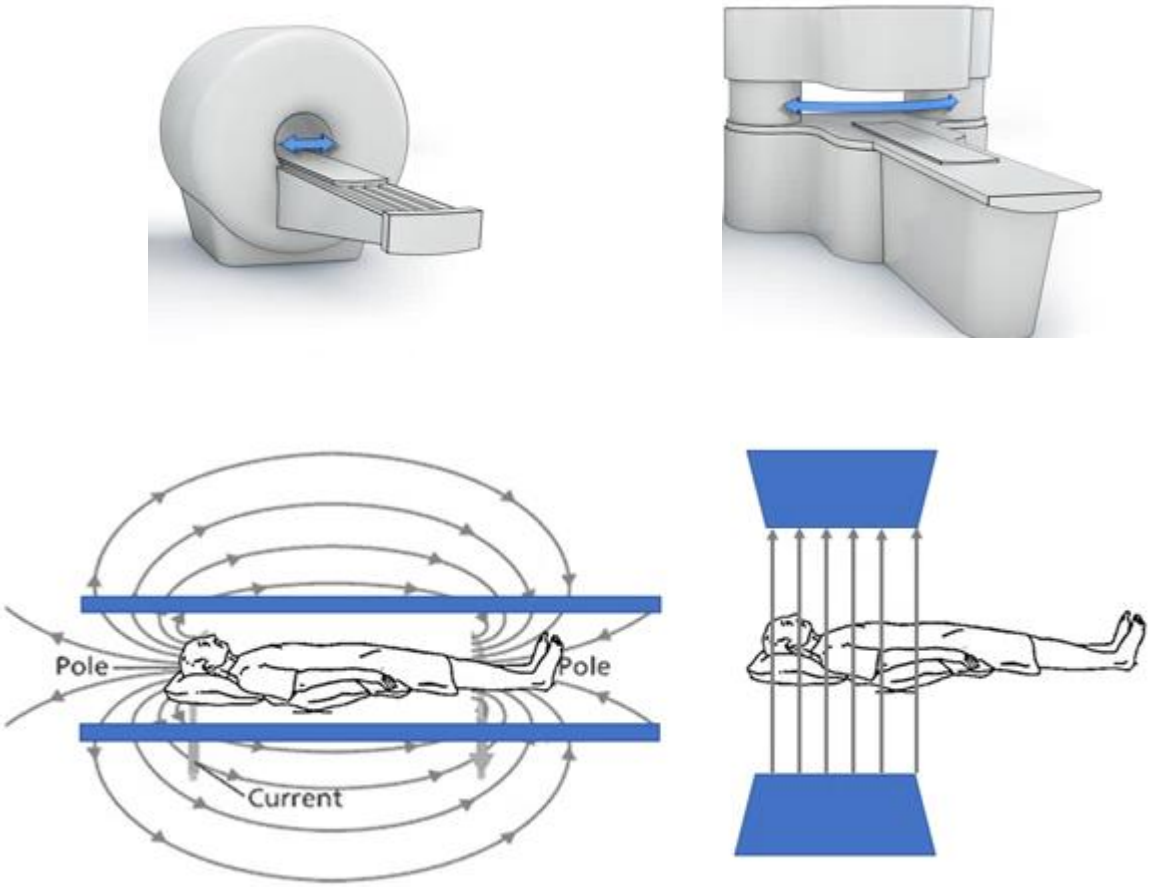

a. Cylindrical scanners b. Open bore scanner

Regarding the position, external magnets present a limit on the distances over which the magnetic gradients need to be produced for effective magnetic targeting in deeper tissues, meanwhile implanted magnets present the risks associated with surgical implantation. Moreover, cardiovascular applications include the use of magnetizable stents, this option has shown the promotion of uniform cell capture and complete endothelialization. [12], [14], [74]

Nacev *et al.*[85], analyzed the behavior of magnetic particles under blood flow conditions in an idealized straight channel in presence of uniform magnetic forces. They considered advection, magnetic and diffusion forces as the main forces acting upon the magnetic

particles and they identified three typical behaviors: blood velocity dominated, magnetic force dominated, and boundary layer formation.

Afterwards, different studies have emerged to identify which variables increase the capture effectiveness when the magnetic force is prevalent. Mirzababaei *et al.* [86], studied that efficiency in an aneurysm model under the effect of a bipolar magnetic system. They demonstrated that blood flow velocity is inversely proportional to the capture efficiency; this implies that as the fluid velocity increases; the enhanced hydrodynamic drag force acting on the particles overcomes the exerted magnetic force on the particles.

Previously, Sharma *et al.* [87], had exposed that the velocity of blood and magnetic particles are appreciably reduced under the influence of magnetic field. This implies that even at low magnetic field strengths, a considerable amount of magnetic capture will occur.

Numerically, the capture efficiency η of magnetic particles by an imposed magnetic field is calculated by the ratio between the number of inserted particles and the total number of the released particles on the vessel walls, as presented in Eq.(3-1) where n_{in} is the number of particles arriving and n_{out} the number of particles leaving [40], [43], [74], [77].

$$\eta \equiv \frac{n_{in-}n_{out}}{n_{in}} \tag{3-1}$$

Another relevant variable for capture efficiency is the injection point of the particles. Kayal *et al*. [88] identified that under strong magnetic fields, the MNP tend to glide along the wall of the channel before reaching the targeted region and suggested to set the injection point near to the target area. However, administration of a near-target injection is medically hazardous in many cases [35].

The success of therapeutic targeting is also related with the multiple nanoparticle interaction. According with MDT, the magnetic force depends on the volume of the magnetic particle. It is notable how the particle size and coating influence the particle behavior within biological systems, the close proximity of these particles reduce the

average drag force per particle, making the entire cluster easier to magnetically trap and steer [4], [11], [34].

It is known that the shape of the particles also affects their magnetic properties, however most of the researches have been made with spherical particles, and there is a lack of comparisons with non-spherical models [34], [37][38].

Hajiaghajani *et al.* [89], created an algorithm to find the required magnetic force for magnetic drug targeting in human muscular arteries. They found that magnetic coil specifications influence the type and strength of magnetism. In addition, Patrick *et al* [90], linked the iron oxide core size and composition with the produced magnetic force.

In the current state of the art created for this thesis, nothing has been found regarding the effectiveness of the magnetism targeting on wide neck stented saccular brain aneurysm and there is a lack of knowledge on the variables that influence the most the endothelial magnetic labeled cells capture efficiency.
These findings support the interest of studying the link between the blood flow dynamics with the magnetic targeting to promote total occlusion in wide neck saccular brain aneurysm, based on the hypothesis that cells will be attracted and maintained to promote the tissue growing.

4. In silico studies: Computational Fluid Dynamics

Blood flow and related phenomena can be described using partial differential equations. Due to their complexity, they are approximated and solved using discretization methods and small domains, leading to appropriate numerical solution, where the results are valid at discrete locations in space and time.

During the last decade, the convergence of medical imaging and computational modeling technologies, has enabled tremendous progress in the development and application of image-based computational fluid dynamics modeling of patient-specific blood flows. At present, Computational Fluid Dynamics (CFD) is the basic technology used for providing estimations of the hemodynamic flow behavior in intracranial aneurysms, in combination with the real data included in the numerical blood flow simulations, it allows the achievement of more realistic and accurate results [91]–[93]. However, as part of the understanding the physical world with fast computations, some simplifications are always required on the models in terms of flow conditions, geometry and/or blood properties [94].

This chapter describes the current state of the art of CFD simulations of wide-neck saccular brain aneurysm, focusing in the hemodynamics changes related with FD placement and cell therapy using magnetic fields; it reviews important findings, discusses the CFD simulations, limitations, and opportunities for further research. It is remarked that the understanding of the interaction between magnetic field strength, flow conditions, particle injection point and particle geometrical features, is important to be considered when endothelial cell attraction and attachment is studied to promote vascular tissue regeneration.

4.1 Magneto-hydro-dynamics (MHD) and Ferro-hydro-dynamics (FHD) numerical models

Cells manipulation inside the blood flow occurs when the fluid forces are overcome by the magnetic field strength [9], [19], [95], [96].
To describe the changes in the flow conditions on a saccular brain aneurysm due to the presence of a uniform magnetic field, different mathematical models have been presented in literature considering blood as an electrical or non-electrical conducting fluid

The behavior of electrical conducting fluids under magnetic fields can be modeled using magnetohydrodynamics (MHD) approach. In this model, electrical currents are induced in the moving electrically-conducting fluid when this fluid is subjected to a transverse magnetic field. The interaction between these induced currents and the exerted magnetic field generates a resistive type force called Lorentz force. This force tends to retard the flow and affects the characteristics of temperature field [76], [97].

According to the above mentioned considerations the governing equations of flow for an incompressible, homogeneous, non-Newtonian biofluid are represented coupling Navier-Stokes and Maxwell governing equations where both electric conductivity and magnetization appear in the momentum equation source terms as shown in (4-2).

- **Continuity equation**

$$\nabla \cdot V = 0 \tag{4-1}$$

- **Momentum equation**

$$\frac{\partial \mathbf{V}}{\partial t} + (V \cdot \nabla)V = \mu \nabla^2 \mathbf{V} + \frac{1}{\rho}\left[-\nabla p + (J \times \mathbf{B}) + \mu_0 (M \cdot \nabla)H\right] \tag{4-2}$$

As mentioned before, if the fluid is electrically sensitive, the magnetic field generates a Lorentz force on it, where the current intensity J, in absence of the electric field, is derived from the Ohm's law shown in Eq. (4-3).

$$J = \sigma(u \times B) \tag{4-3}$$

Conversely, considering the blood as an non electrically conducting fluid, the mathematical model that describes the magnetic behavior is called Biomagnetic fluid dynamics (BFD) and was developed by Haik *et al*. [98]. This approach, derived the mathematical model based on the principles of Ferro hydro dynamics (FHD) where it is ignored the effect of polarization and magnetization and the induced current is negligibly small. In this sense, the Lorentz force is not present, and the electric field does not influence the fluid behavior [97]. For weak magnetic conductor materials, such as blood, it has been suggested that FHD approach can be used without losing accuracy and reliability [62], [99]–[102].

In the FHD approach, when blood is placed in a magnetic field H, a magnetization M (magnetic moment per unit volume) is induced, which is related to H by the Eq. (4-4).

$$M = \chi H \tag{4-4}$$

Here magnetic susceptibility χ indicates the degree of magnetization of the material in response to an applied magnetic field. This equation is valid when *M* is aligned with the applied magnetic field H.

In the absence of an existing magnetic moment, it should be noted that the magnetic field H can be related to the magnetic flux density B by Eq. (4-5) or in SI units by (4-6)

$$B = \mu H \tag{4-5}$$

$$B = \mu_0(H + M) \tag{4-6}$$

where μ is the magnetic permeability and can be define in term of magnetic permeability in vacuum μ_0 by Eq.(4-7)

$$\mu = \mu_0(1 + \chi) \tag{4-7}$$

The main difference in FHD approach is the momentum equation, presented in Eq. (4-8), where the Lorentz equation is not present

- **Momentum equation for FHD**

$$\rho \frac{\partial V}{\partial t} = -\nabla p + \mu \nabla^2 V + \mu_0 (M \cdot \nabla) H \tag{4-8}$$

The last term $\mu_0 (M \cdot \nabla) H$ in Eq. (4-8) represents the influence of the magnetic field as a body force on the fluid element due to fluid-magnetic pressure.

Blood as a ferrofluid is composed of magnetic nanoparticles suspended, its behavior can be understood by studying the details of the blood flow through arteries with particles vs bulk blood under magnetic field. It means that its behavior can been modeled as a single-phase or two-phase fluid depending on the research interest [96], [103]–[105]. In medical science, biomagnetic fluids are considered as a working fluid. These types of fluids are a part of physiological fluids, which their flows are affected under the influence of magnetic fields and its effects on the pressure and velocity at the target site can be analyzed as the change of the magnetic intensity [85], [104].

4.2 Cell responsiveness to the magnetic forces

Beside understanding the behavior of the carrier fluid, it is important to predict the transport and capture of the discrete phase, in this case, the magnetic particles migration under the influence of magnetic field. It has been shown that under the influence of an applied magnetic field, the particle seeks to reduce its energy by moving towards the magnetic field source, thus particle motion is driven by the magnetic flux density, rather than magnetic field strength [62], [106].

There are two methods of describing fluid motion, Lagrangian and Eulerian. In the first one all fluid particles are followed, and it can be described the variations around each fluid particle along its trajectory. In the second one, the variations are described at all fixed stations as a function of time. In addition, two different approaches are available for the particle analysis: One-way and Two-way Particle-fluid Coupling. In the first approach the motion of the particles is impacted by the fluid flow due the effects of viscosity via drag and turbulence, but the particle motion does not alter the flow. On the other hand, in the

two way approach there is a transfer of momentum, mass or energy from the particles to the fluid [107].

Once the velocity field of the carrier or continuous fluid becomes available using the Eulerian treatment, the discrete particle motion can be numerically integrated with the kinematic velocity. This particle flow is modeled by a discrete phase model (DPM) that utilizes a Lagrange treatment to provide average fields within an Eulerian granular framework. [78], [107], [108]

Euler-Lagrange model treats the blood as a continuous fluid by solving Navier-Stokes equations, and the dispersed solids as an interpenetrating continua by tracking a large number of particles [109]. A fundamental assumption made in the Euler-Lagrange approach is that the dispersed second phase occupies a low volume fraction, less than 12% of the total volume.

To evaluate the effects of applied magnetic fields over the particles, it is required to simulate the particles as a variable concentration continuum that moves at the local fluid velocity in conjunction with the magnetic hydrodynamic model (MHD) [110].

The equations that represents the phenomenon for the mixture, are continuity Eq. (4-9) and the source term DPM force is included in the momentum Eq (4-8), resulting Eq.(4-10). Finally, for the particle concentration, a scalar transport Eq (4-11) represents the advection/diffusion equation.

- **Continuity equation**

$$\frac{\partial}{\partial t}\rho + \nabla \cdot (\rho\, V) = 0 \tag{4-9}$$

- **Coupled FHD and momentum equation**

$$\rho\left(\frac{\partial V}{\partial t} + (V.\nabla)V\right) = -\nabla p + \eta\nabla^2 V + \mu_0(M \cdot \nabla)H - F_{DPM} \tag{4-10}$$

- **Advection/diffusion equation.**

$$\int_v \frac{\partial c}{\partial t}\, dV + \int_S cV\, dS = \int_S (D_{Brown} - D_{Blood})\, \frac{\partial c}{\partial x}\, dS \tag{4-11}$$

The right hand side of the momentum equation (4-10) is a sum of all the forces acting on the control volume: pressure, gravitational force, bulk magnetic force applied by an external magnetic field gradient, viscous force, and interparticle magnetic force (4-12).

$$F_{DPM} = \nabla \rho_m c_p (1 - c_p)(V_p + V_f) \tag{4-12}$$

Particle Trajectories

In a cluster of magnetic particles, every particle behaves like a magnetic dipole and interacts with every other particle. The specifically forces that act on the magnetic particles can be studied such us magnetic forces, hydrodynamic drag forces generated by the blood flow, gravitational forces, buoyancy forces, and inertial forces.

$$m_p \frac{dV_p}{dt} = F_m + F_s + F_b + F_{g\ldots} \tag{4-13}$$

where V_p and m_p are the particle velocity and mass. The right-hand side represents the forces that affect the particle like drag force F_s, magnetization forces F_m, Buoyancy F_b and gravitiy F_g.

The drag force is defined by the Stokes expression in Eq. (4-14) where V_p and V_f are velocity of the particle and fluid respectively, μ is the viscosity of the carrier fluid and D_p is the particle diameter.

$$F_s = 3\pi\mu D_p (V_p - V_f) \tag{4-14}$$

The magnetization force F_m, also known as the Kelvin force or magnetophoretic force, on a magnetized particle of volume V is given by Eq. (4-15).

$$F_m = \iiint_{Vol} \mu_0 (M \cdot \nabla) H \, dV \tag{4-15}$$

The magnetization of such particles can often be assumed approximately proportional to the applied magnetic field, as presented in the Eq. (4-4).

When the magnetic field is approximately constant over the volume $\pi {D_p}^3/6$ of a spherical particle with diameter D_p and the particle's surrounding medium has a negligible magnetic susceptibility, the magnetization force F_m can be expressed by Eq. (4-16). Where μ_0 is the magnetic permeability of vacuum.

$$F_m = \pi {D_p}^3/6\, \mu_0 (M \cdot \nabla) H \tag{4-16}$$

In addition, the magnetization force F_m acting on particles shown in Eq (4-16) can be expressed in terms of magnetization presented in Eq. (4-8) and the volume of the particle v_P. As shown in Eq (4-17)

$$F_m = v_P \mu_0 (M \cdot \nabla) H \tag{4-17}$$

Finally, particle velocity V_p assuming that the particle inertia can be neglected, is estimated as a sum of the fluid velocity V_f and a magnetic velocity V_m Eq (4-18). Where V_m shares the direction of the magnetic force. It can be expressed in terms of F_s as shown in Eq (4-19)

$$V_p = V_f + V_m \tag{4-18}$$

$$V_m = \frac{F_m}{3\pi\mu D_p} = u_0 \left(\frac{F_m}{F_s}\right) \tag{4-19}$$

To ensure that ferromagnetic nano-particles do not obstruct the flow within a blood vessel, the phenomenon requires a dilute suspension (0.1% volume fraction) of μm scale particles suspended in blood moving through arteries that are large relative to blood cells. Taking into account that the particle volume fraction considered is always less than 1%, it could be assumed that the mixture is incompressible.

In addition, for cells fishing process, it could be assumed that all particles have the same magnitude and direction of dipole moment since particles are under the influence of a strong, uniform external magnetic field.

In this particular case, the homogeneous flow model requires that the particle Stokes number described in (4-20) be very small so that the particles move at the same velocity as the blood plasma immediately surrounding them making them responds almost instantaneously to accelerations of the flow around it. The expression of the stoke number includes the particle density ρ_P, diameter d_P , the artery diameter D, blood viscosity μ and and the bulk velocity calculate with the fluid velocity V_f and the particle velocity V_P

$$St = \frac{\rho_P {d^2}_P (V_f - V_P)}{9\mu D} \ll 1 \quad (4\text{-}20)$$

Different variables such us trajectories of magnetic nanoparticles, particle residence time (PRT) and particle deposition, are typically calculated in the Lagrangian approach, where a large number of particles are seeded in the flow, their individual trajectories are computed, and the time spent by a particle in the domain is calculated. [80], [95], [105].

Reza Habibi & Ghasemi [111] studied accumulation of magnetic nanoparticles near to the magnetic source until it looks like a solid object. The accumulation of nanoparticles is due to the magnetic force that overcomes the fluid drag force. As the magnetic strength and size of the magnetic particles increase, the accumulation of nanoparticles increases, as well. The magnetic susceptibility of particles also affects the flow field and the contour of the concentration considerably.

Khashan *et al* [107], studied particle capture using one-way and two way particle-fluid coupling analysis. They found that for lowest volume fraction the calculated trajectories have not significant changes to those obtained using one-way coupling. For higher volume fraction, it is produced higher capture efficiency because of a cooperative effect between the particle motion and flow.

4.3 . Geometric models

Because most intracranial aneurysms are saccular and taking into account the most common location of the Brain Aneurysm [27], [31], [112], the geometry of interest in the study is a Saccular Brain Aneurysm at the anterior communicating artery (ACoA).

The computational blood flow simulation starts by defining the physical bounds of the artery. Where the accurate of the numerical results are related with the correct geometry representation. Despite in recent years patient-specific geometries have been widely used, the understanding of the flow dynamics under new phenomenon can be studied using idealized geometric models. It is the starting point that allows to isolate the effect of geometry on the overall hemodynamics analysis.

Some authors have considered the influence of the geometry on the hemodynamic simulation. Besides the fluid volume, related with aneurysm morphology, some studies regarding the artery walls have been presented. Specifically, it is known that once the aneurysm is formed, the dilatation on the wall produces a reduction on the wall thickness in the dome [113], [114]. Valencia *et al.* [115], studied the effect of taking into account this change on the geometry on the aneurysmal wall displacement and effective stress. They found that both variables depend on wall thickness and wall model especially at systole. Torii *et al.* [116] reported differences in hemodynamics depending on wall thickness on a patient specific 3D model. They evaluated the influence of wall thickness on fluid–structure interaction in the Velocity Profile & WSS & Pressure in wall. Years later, Voss *et al*. [114], presented a patient specific simulation of a saccular aneurysm. They highlighted the importance of proper geometry reconstruction and accurate description of local wall thickness regarding hemodynamic FSI simulations since it plays an important role for the prediction of stress distributions inside aneurysm walls.

As shown previously the difference in the thickness after the vessel deformation has an incidence on the hemodynamic performance and should be considered in the aneurysm treatment simulations. In addition to the thickness consideration, one simplification of the geometry study domain have been reported by Lee *et al.*, [117] who study the effect of the length of the model on hemodynamic and mechanical variables, aneurysm volume and cross-sectional area. Their findings support the idea that using short elastic upstream artery can shorten the time required for patient-specific FSI simulations without impacting the overall accuracy of the results, which avoid to simulate large models.

Finally, the geometry of the domain includes the presence of a stent. The simulation of exact replicas of stents is not necessary, because it implies time consuming CAD

modeling, meshing and long computation time. Rather, it is recommended to carry out simulations using porous layers to represent the stents in the neck region. They are able to predict qualitatively and quantitatively the hemodynamics in stented aneurysms [58], [118]

4.4 Discretization and meshing schemes

Depending on the computational mesh used for the fluid domain, the spatial discretization of the computational domain defines the computational numerical methods into: fixed mesh methods, moving mesh (boundary-fitted mesh) methods, and mesh-free methods.
The fixed mesh methods likewise can be classified into structured (hexahedral) or unstructured (tetrahedral) meshes [7]. Depending on the complexity of the geometry and the phenomenon that is intended to be evaluated any of those options can be selected or a combination of both.

Caballero *et al.* [94] indicated that, for symmetric geometry like the curved tubes, structured meshing are the preferred option. Meanwhile more complex geometries like patient-specific simulations are accurately modeled using unstructured meshes with tetrahedral, prismatic and pyramid elements.
Among the challenges in the CFD simulation of stented aneurysms, there are major difficulties related to the meshing of stents. To this sense some simplifications are performed like modeling the stents only at the neck of the aneurysms [119]. Lopez [58] compared the performance of spiral, mesh stents and porous medium method to simulate the case of multiple FD treatments and identified that the geometry modeling problem can be simplified by using porous media stents, and the results of the simulations are comparable with the helix and mesh models. In addition, Zhang *et al*. [7], used also a porous medium zone with equal flow resistance to simulated the FD stents and estimated the dynamic and resistance forces related with the stent presence by performing adaptive meshing refinement near the stents.

4.5 Material properties

Blood

Human Blood is a time-independent non-Newtonian fluid conformed by plasma with Newtonian behavior and cells that changes the blood viscosity with a strong shear rate dependency.

Jeon *et al.*, [59] studied the influence of non-Newtonian properties of blood in an idealized arterial bifurcation model with a saccular aneurysm, and showed that in the regions with relatively low velocities there is no essential difference in the results with both fluid models. With the same consideration, several authors have presented CFD simulations using Newtonian behavior due to the size of the brain vessels [120]–[122].

However, depending on the physiological conditions intended to simulate, hemodynamic simulations require constitutive models that can accurately capture the rheological response of blood. For example, when cell separation from the blood are studied under hemodynamics conditions, it has been showed that when the magnetic field is acting, the fluid viscosity increases, so the rheological properties of blood can significantly affect the flow and particle phenomena showing a difference in a Newtonian and non-Newtonian model [62], [101], [123].

In the magnetic study it is relevant to understand the viscosity effects on the hemodynamics and more complex blood constitutive models should be used [80], [123].

Most of the rheological models proposed in the literature to predict the stress vs. strain rate relationship of blood fall into two categories: Models that predict shear-thinning effects and models that exhibit yield stress.

The first category includes the Cross model, the non-Newtonian Power law model, the Carreau model presented in Eq (4-21) and the Second-grade model. On the other side, models that exhibit yield stress includes the Casson model and the Herschel–Bulkley model [55] [124].

Campo-Deaño *et al*. [55] have experimentally studied the viscous properties of blood and compared the experimental results with the non-Newtonian conventional models. Their

comparison showed that Herschel-Bulkley Eq. (4-22) and Carreau models Eq. (4-21) have a good agreement with the experimental data, being Herschel-Bulkley the best agreement.

Carreau model equation (4-21)

$$\mu_{\text{eff}}(\dot{\gamma}) = \mu_{\text{inf}} + (\mu_0 - \mu_{\text{inf}})(1 + (\lambda\dot{\gamma})^{a\frac{n-1}{a}} \quad (4\text{-}21)$$

Where $\mu_{inf} = 2.2 \times 10^{-3}\ Pa\ s$ is the Infinite Shear Viscosity , a is an empirical constant a = 0.644, $n = 0.392$ is $\lambda = 0.11(s)$ is the time constant and $\mu_0 = 22 \times 10^{-3}\ {}^{\text{kg}}/_{\text{m s}}$ is the Zero Shear Viscosity for healthy blood.[125]

Shear rate dependent Herschel-Bulkley model Equation (4-22) [57]

$$\eta = k\dot{\gamma}^{n-1} + \left({}^{\tau_0}/_{\dot{\gamma}}\right) \quad (4\text{-}22)$$

Where $k = 8{,}9721 \cdot 10^{-3}\text{N}\,s^n/m^2$ is the Consistency Index, $n = 0.8601$ is the Power-Law Index and $\tau_o = 0.0175\ N/m^2$ is Yield Stress Threshold for healthy blood.

- **Magnetic blood properties**

The most characteristic biological fluid is blood, due to its composition it behaves as a magnetic fluid with a complex interaction of the intercellular protein, cell membrane and hemoglobin that makes it sensitive to magnetic perturbation. Moreover, its magnetic properties are affected by factors such as the state of oxygenation blood becomes diamagnetic if oxygenated and paramagnetic if de-oxygenated [101], [126].

Experiments presented in literature demonstrated that the electrical conductivity of blood depends on its velocity, i.e. the electrical conductivity of moving blood is higher than for the stationary one [81]. The measured electrical conductivity σ of flowing blood is reported between 0:7 and 0:9 S/m [81], [97], [127]

Through the human body, magnetic fields propagate essentially unchanged because the magnetic susceptibility of tissue is close to zero χ≈10^{-6}
The magnetic susceptibility of blood is about $\chi = -3.5x10^{-6}\ and\ \chi = -6.6x10^{-7}$ for the deoxygenated blood in vein and oxygenated blood in artery, respectively [76], [101], [126]

- **Wall vessel**

In the study of near-stent hemodynamics, several authors have evaluated the impact of the flow diverting device assuming vessel walls as well as the flow-diverting devices to be rigid [7], [10], [58], [128], [129]. However, all of them agree that one approach to solve the limitation of considering rigid wall in CFD simulations is to simulate fluid–structure interaction (FSI), and overcoming the lack of proper specification of intra-arterial pressures and distributions of vessel wall properties like elasticity and thickness, makes it feasible [94].

Furthermore, the isotropic and anisotropic mechanical behavior of the tissues has been studied, due to the three-layer structure where the collagen fiber strength and orientation and the surrounding tissues change the vessel wall properties. Lozovskiya *et al*. [113] presented that the integrity of the aneurysm wall is dependent not only on the actual strength and elastic stiffness of the fibers, but also on their distribution and the direction in which they are aligned. However, despite the highly non- linear and anisotropic mechanical behavior of the artery, it has been shown that the fluid dynamics is not strongly affected by using isotropic constitutive models [8], [124], [130]–[132].

It is known that the arteries are dilated by blood pressure due to the soft and flexible structure of vessels in a not linear way, rendering it necessary to include the hyperplastic models, describing both material nonlinearity and large deformation [131], [133]. Valencia and Solis [115] presented the FSI study on an idealized brain basilar aneurysm on a bifurcation with homogenous wall thickness. They identified that the wall thickness, the Young's modulus in the elastic wall model and the hyperelastic Mooney–Rivlin wall model affect the aneurysm deformation and effective stress in the wall especially at systole.

Brain vessels can be seen as compressible hyperelastic solids, consequently, multiple authors have simulated the vessels using a five-parameter hyperelastic Mooney-Rivilin

model [124], [130], [134], [135]. These models describe that for a given strain, the stress state is determined as the derivatives of the strain energy density with respect to the strain components as presented in [136].

Depending on the physical models intended to simulate FSI can be one, two or three-way coupling. The pulsating blood flow inside an elastic vessel can be seen as a two-way coupling FSI, since it includes the interaction between fluid flow and elastic material. In addition this case is a surface-coupled multiphysics problems since the coupling is acting at the interface between the two subproblems fluid and solid [137].

To describe the interaction between blood and vessel, there are three coupling conditions that are included on the boundary conditions of each subproblem: (i) kinematic, that describes velocity continuity at the solid and fluid interface (ii) dynamic that express normal stresses continuity of fluid and solid and (iii) geometric conditions that avoid the hole presence in the fluid-structure interface [137].

In the ALE formulation the fluid and solid domains are allowed to move to follow the distensible vessels and deforming fluid domain in that sense the mesh is deformed dynamically to always conform to the boundaries of the computational domain, requiring the continual update of the geometry of the fluid and the structural elements. [110], [124].

The Dynamic Mesh method allows the two-way data transfer of the fluid and solid domain solvers by sharing the stress distribution on the interface wall displacement and the wall displacement and volume changes that results from the solution of the fluid and solid domain respectively [138].

- **Endothelial Cells labelled with Magnetic nanoparticles.**

As presented before, most common MNPs used for cell labelling are made from magnetite. It is a paramagnetic material that by definition has a permanent magnetic dipole moment. However, these permanent magnetic dipoles never line up spontaneously. In the absence of any applied external magnetic field, they are randomly aligned. However, when we place a paramagnetic material in an external field, the dipoles experience a torque that tends to align them with the field, thereby producing a net

magnetization. This is plausible because without the external field there would be no alignment of dipoles and hence no magnetization

Magnetite cores (e.g. Fe3O4) of ferromagnetic particles have magnetic susceptibilities 5–7 orders of magnitude higher than that of tissue $\chi \approx 20$ therefore these particles are strongly influenced by magnetic field [85]

4.6 Boundary and initial conditions

As all the CFD models, blood simulations on cerebral aneurysm requires detailed information of the real phenomenon, to define if the simulated fluid will mimic the physiological conditions. However, patient-specific measurements data is not always available to be included on the computational simulation, therefore acceptable assumptions are usually made on the boundary and initial conditions.

Some studies have been developed regarding the influence of different boundary conditions (BCs) on CFD analysis for intracranial aneurysms [31], [139], [140]. Pereira *et al* [139], compared Digital Subtraction Angiography (DSA) sequences with the results of CFD analysis with different inlet BCs applied to IA, showing that dynamic pressure loss was not affected with the different inlet BCs while WSS showed differences. Liang *et al* [31] compared the ACoA aneurysms hemodynamic features with generic and patient specific BCs. They found that intra-aneurysmal flow patterns and WSS are significantly different, and remark the importance of having patient-specific BCs when modeling a ACoA aneurysm.

Recently, in a pursuit of having patient specific data, Guerra *et al* [141], proposed Data Assimilation method to reconstruct blood flow profile to be used in CFD simulations, once these information is not always available. They showed accurate reconstruction of the velocity profile even working with noisy data on realistic and idealized geometries domains.

Most common boundary conditions for blood simulations on IA aneurysm are: inlet boundary, vessel wall boundary, outlet boundary and prescribed pressure. Main aspects are further discussed.

- **Fluid Inlet boundary *c*ondition**.

Velocity boundary condition is usually prescribed at the inlet for IA simulations. When the information is available, a based on patient-specific time-varying velocity data obtained with PC-MRI or ultrasound is included, otherwise different idealized profiles have been used, such us: fully developed (parabolic), flat (plug) or Womersley flow pattern [115], [121].

Inlet boundary condition in transient IA studies is a flat velocity profile used together with a pulsatile waveform, usually this inlet boundary condition have been predicted by a 1-D model of the cerebral arterial network. [31], [94].

Pulsatile waveform: As presented in **Figure 4-1**, during a cardiac cycle blood flow is unsteady, where it is possible to distinguish pulsatile conditions between diastole and systole in all arteries. This pulsatile phenomenon can be expressed as a variation of the Reynolds number as shown in (4-23)

$$Re(t) = Re_{mean}\left[1 + \sum_{n=1}^{5} A_n \cos\left(2n\pi\frac{t}{T} - B_n\right)\right] \quad (4\text{-}23)$$

Figure 4-1: Physiological waveform in the human right coronary artery [142]

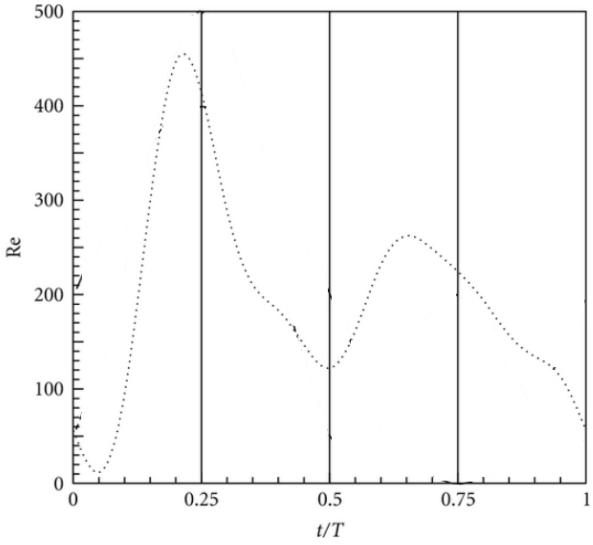

- **Vessel wall boundary.**

This boundary represents the interface between the fluid domain and the vessel wall. In the physical world, the cerebral aneurysm boundary is lined by a layer of endothelial cells, these layers are enforced to no-slip condition, equal tangential fluid velocity and wall velocity, zero normal velocity component and shear stress can also be specified.

In addition, the simulation of blood flow dynamics in intracranial aneurysm cannot be isolated from the rest of the cardiovascular system, making necessary to consider the Cerebral Spinal Fluid [58], [115], [135], [143].

Aranda-Iglesias *et al* [135], included the cerebral spinal fluid as a incompressible and Newtonian fluid in the outer surface of the aneurysm and calculated the total pressure exerted by it on the outer surface of the aneurysm.

Regarding the magnetic studies, the walls are usually assumed as an insulating state under the applied magnetic field. The insulating wall is used for boundaries where there is no electric current going through the boundary [111], [127], [144], [145].

During the interaction with the DPM model the discrete particles can interact with the walls with different BCs. DPM can Reflect, be trapped, escape or create a wall film, which is intented to model particles absorption into a wall film once they hit the wall. The discrete particles can also splash creating additional particles.

Fluid Outlet boundary.

For cerebral aneurysm hemodynamic simulation, the analysis is limited to a certain domain, being not necessary to trace all the branching to reproduce physiological conditions, with that consideration, some simplifications can be afforded resulting in several outlet BC possibilities, like open BC, fully developed assumption or resistance BC as presented in [55].

It is also possible to represent the wave propagation and artery fluid impedance representative of the downstream vasculatures, where multiple outlets can be simulated. This method requires an expensive simulation since several cardiac cycles are required [55], [140].

In their study, Chabannes *et al.* [140], presented a review of the actual effects of different modeling assumption in the cerebral venous network hemodynamics parameters, they conclude that outflow treatment has a less impact on the results comparing with inlet BCs changes.

- **Magnetic boundary conditions**

Boundary conditions can be set to cell zones and wall boundaries. In cell zones, the conditions are defined from the material properties like the electrical conductivity and magnetic permeability. For wall boundaries, the boundary condition can be set as an Insulating Wall, Conducting Wall, Coupled Wall or Thin Wall [146]

- **Particle motion and interaction conditions**

Boundary conditions are defined to describe how particles interact with other zones and how they eventually leave the model.

5. Materials and methods

Specific aims are developed in two phases. First, an *in silico* study is performed to describe the effects of applying uniform magnetic fields on the behavior of the blood flow inside the sac of an idealized intracranial wide-neck saccular aneurysm. Because most IA are saccular, this project is focused on this type of aneurysm.

In the second phase, a disperse phase model is used to simulate magnetic label endothelial cells injected in the blood. Additionally, a virtual stent is positioned in the 3D aneurysmal model, aimed to trap the particles of the domain. The number of trap particles is used to calculate the cells targeting efficacy.

As previously presented in 3.2, magnetic fields available for targeted particle delivery can have configuration differences in the frequency, amplitude and direction. The influence of aforementioned magnetic field configurations on the number of trap endothelial cells is studied and compared to classify the factors incidence over the magnetic cells targeting efficacy.

In all the *in silico* studies, the geometry is modeled using SOLIDWORKS software V16.0 [147]. After, Computer-aided design (CAD) model is imported and meshed using ANSYS V16 [148]. The Mesh Quality Inspection Tool is used to check errors or warnings, before mesh files are used in the simulations. Mesh-independent analysis is performed.

Computational simulations are performed in a work station computer 32 GB RAM memory using Finite Volume Method (FVM) in ANSYS FLUENT software [149]. The geometric configuration, mesh generation, material properties, boundary conditions, and governing equations are individually described, based on the results previously presented in literature.

5.1 Hemodynamic changes on a wide-neck aneurysm under the presence of a uniform magnetic field.

The hemodynamic changes are simulated on a wide-neck idealized aneurysm under physiologically realistic pulsatile conditions in a non-Newtonian, transient, CFD three-dimensional model. Three different uniform magnetic fields are applied to the model. Hemodynamic variables are obtained from the idealized model with and without the presence of magnetic field. Values are compared among simulations and with previously reported in literature. The model is firstly validated by other computational work in literature.

The bibliographical review allows to propose the representative geometrical configuration and the boundary conditions needed for calculating the disturbed blood flow parameters. The strength of the magnetic field is varied so as to evaluate its effect on the flow velocity, pressure and WSS. Three consecutive unsteady pulsatile flow cycles are defined in the inlet. Results are reported for the third cycle.

5.1.1 Geometrical configuration

As presented in Figure 5-1, an idealized 3D model of a Saccular Brain Aneurysm of the anterior communicating artery (ACoA) with a curvature of 60º is reconstructed, taking into account the most common location of the pathology [129], [150]. The geometry for the analysis has the dome-to-neck ratio <1.5, defined for wide-neck aneurysms [2]. Both perpendicular height and neck diameter are 5 mm and the aspect ratio (depth/neck width) of 1. Parent vessel diameter is set to 4mm and to ensure that the flow profile is fully developed, the proximal section of the parent artery is set to $10D$, resulting a length L of 40 mm.

Figure 5-1: Idealized 3D model of a Saccular Brain Aneurysm

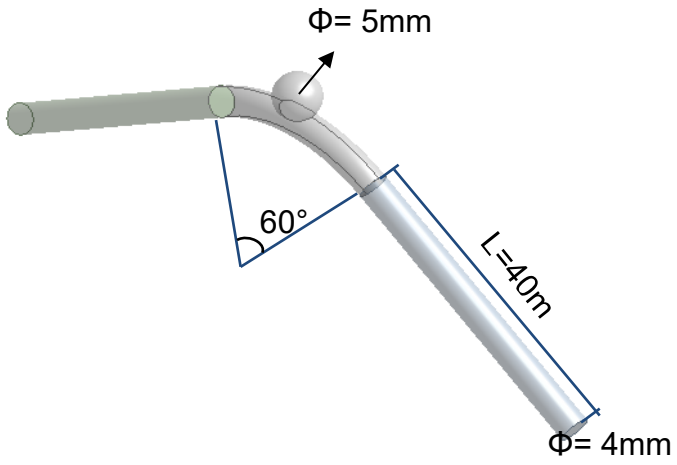

5.1.2 Blood Properties

The density of blood is set to ρ_f= 1050 kg/m^3, magnetic permeability of vacuum $\mu_0 = 4\pi\, x\, 10^{-7}\, {}^{H}/_{m}$ and a Non-Newtonian rheological behavior [151]. Herschel–Bulkley model is considered for the dynamic viscosity μ_f that varies according to Eq (5-1). Where $k = 8{,}9721 \cdot 10^{-3}\mathrm{N}\, s^n/m^2$ is the Consistency Index, $n = 0.8601$ is the Power-Law Index and $\tau_o = 0.0175\ N/m^2$ is Yield Stress Threshold [57].

$$\eta = k\dot{\gamma}^{n-1} + \left({}^{\tau_0}/_{\dot{\gamma}}\right) \tag{5-1}$$

5.1.3 Boundary and initial conditions

Total cerebral blood flow (tCBF) has been reported to be 616 to 781 mL/min in healthy subjects [152]. In their study Zarrinkoob *et al* [153], have evaluated the distribution of tCBF in a Healthy Circle of Willis, founding a 11±4 % passing through ACoA. Pulsatile waveform for the inlet velocity condition in the fluid domain reported by [57] is specified. The duration of each pulse is defined to be 1 second and the maximum velocity is 1.5 m/s at 0.18 seconds in accordance with systole [2]. As considered in recent studies, [81], [154] the vessel wall is assumed rigid, insulate under the applied magnetic field, constant

temperature and porous assumption for arterial walls is neglected. The outlet is modeled as an open boundary with zero static reference pressure since the model is extended 10D after the domain of interest. No-slip condition is set on the vessel wall.

5.1.4 Numerical approach

Navier–Stokes equations are solved to simulate the laminar, transient and incompressible blood flow, coupled with MHD equations. In addition to continuity Eq. (4-1), the magnetization force acting on the fluid is included in the momentum Eq (4-2).

Simulation is solved with a pressure-velocity coupling, using the SIMPLEC segregated solution algorithm. In order to compare the effects of the magnetic field in the flow patterns, different magnetic fields (0.1, 0.5 and 1 Tesla) in the positive Y axis are imposed, according with the coordinate system described in the Figure 5-2. The magnetic field acts on the whole segment of the aneurysm blood vessel. The transient simulation is set to 0.005s time steps and 100 maximum iterations. The magnetic effects are included in the model using the Magnetic Hydrodynamics module (MHD) in ANSYS Fluent 16.1

Figure 5-2. Coordinate system

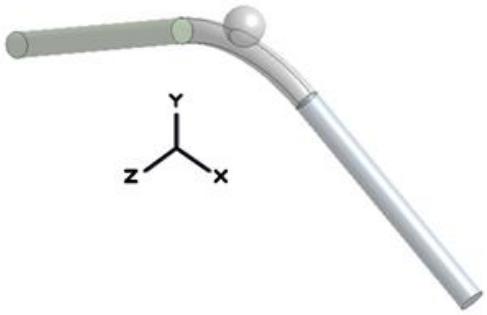

5.1.5 Mesh-independent analysis

In order to define the number of elements that are required in the simulation and to evaluate the mesh quality, a sensitivity analysis is performed to support the theoretical results on the accuracy of the numerical scheme provided before [155] [123].
Skewness parameter is chosen to rate the mesh quality. A skewness less than 0.84 is assumed to be acceptable for the mesh. Highly skewed faces and cells are unacceptable.

After a sensitivity analysis, the spatial discretization of the domain is set to 291705 tetrahedral and hexahedral elements.

The following parameters are set: Residual Root-Mean-Square (RMS) Error values below 10^{-5}, Monitor points for the values of interest have reached a steady solution and there is less than 1% of domain disproportion.

5.2 Influence of magnetic configuration on magnetic cells targeting efficacy

5.2.1 Virtual stent geometrical configuration

Previous studies suggest that hemodynamic conditions play significant role in monocyte adhesion [17], [156]. In this context, since stent implantation changes the arterial blood flow patterns and consequently changes the magnitude and distribution of Wall Shear Stress (WSS), the correct fluid flow characterization should be done in a treated aneurysm. Virtual stenting is performed and hemodynamics is calculated as the starting point both for validating the particle targeting efficacy, under blood flow conditions [45], [157].

This chapter presents the hemodynamics of the brain aneurysm treated with FD, where a helicoidal stent with rounded strut diameter 70 μm, is placed in the neck of the aneurysm. The first model does not consider any magnetic field, in order to elucidate the basal point for the analysis.

According to Lopez [58], helicoidal stents models are more effective in eliminating the inner vortex from the unstented case, making the inner flow less chaotic. As suggested by Bouillot *et al* [118] the virtual stent is reduced to a patch across the IA neck, as presented in Figure 5-3.

Figure 5-3. Helical virtual stent patch in saccular aneurysm neck. a. 3D view, b. bottom view, c. isometric view

a. b. c.

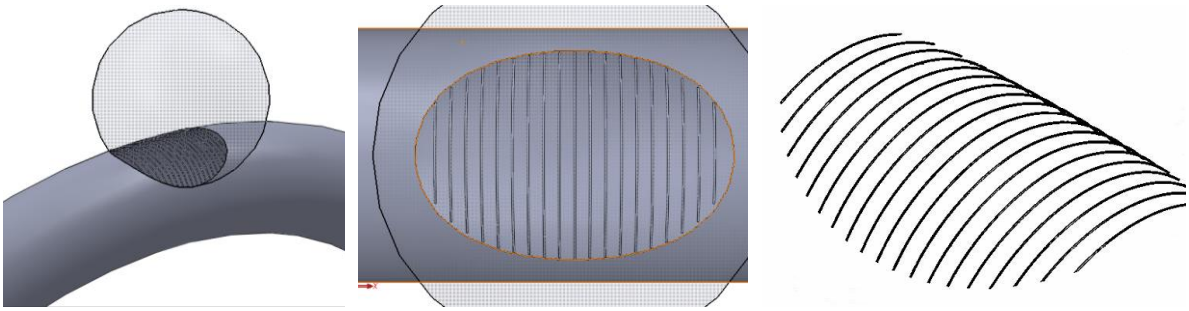

5.2.2 Properties

Blood properties are previously described in section 5.1.2

- **Stent Material**

Magnetic 2205 duplex stainless steel (2205 SS) is used as the stent material, with a relative permeability of 1.4E6 siemens/m to consider the stent conductivity in the magnetic attraction analysis.

- **Discrete phase description**

Under the influence of an applied magnetic field, the particle seeks to reduce its energy by moving towards the magnetic field source as a complete body [69], in this sense, cells, labeled with 29.8pg ± 0.1 pg iron oxide/cell [41], are modeled as spheres with 10 µm diameter. Considering the total volume of the domain, 1,468x10^{-6} m^3, the discrete phase is defined to be 1% of the total volume. That are 14.520 cells to be injected in the domain. With this consideration volume fraction of the second phase is negligible.

Particle magnetic susceptibility can be calculated using Eq.(5-2) [158]

$$\chi = -0.14 d_p . 10^6 + 0.98 \qquad (5\text{-}2)$$

Where, dp is the particle diameter.

Interaction with continuous phase is assumed between the blood and particle flow fields and the interaction between particles is neglected because the particle flow is diluted.

5.2.3 Boundary and initial conditions

10 µm diameter cells are injected with steady Inlet velocity 0 m/s. These initial conditions along with the physical properties of the discrete phase are utilized to initiate trajectory calculations and get the region of interest (ROI), as a homogeneous suspension.

After labeling, cells themselves are considered the magnetic particles. They have a finite magnetic moment, density ρ_{total}, diameter D, volume V_{cell} and mass m_{total}., as describe in Table 5-1.

Table 5-1. Cells properties summary.

Symbol	Description	Magnitude	SI
D_{cell}	Cell diameter	1E-5	m
ρ_{cell}	Cell Density	1055	kg/m^3
V_{cell}	Volume – Perfect sphere	5,2E-16	m^3
m_{cell}	Cell mass	5,5E-13	kg
m_{MNP}	total MNP mass	2,98E-15	Kg
$m_{total\ cell}$	Total mass labelled cells	5,27E-13	kg
$\rho_{total\ Cell}$	New cell density	1060,7	Kg/m^3

Particles are injected in a uniform distribution at the inlet face of the computation domain and tracked through the geometry until they meet one of three fates: (1) trapping on stent surface by collision, (2) escape from the domain through the outlet face, or (3) continued suspension in the flow. The fate of the particles is then recorded and summarized as a particle history file. Details about each boundary condition are described below.

- **Inlet BC**

A steady inflow velocity of 0.7 m/s is assumed as the inlet boundary condition, in concordance with distribution of total cerebral blood flow in the individual arteries study [153] Inlet boundary is 10D away of the region of interest.

For the discrete phase the escape boundary condition is set in inlet surface.

- **Wall BCs**

After virtual stenting, the model is formed by two walls, aneurysm wall where the particles collide and stent wall where particles are trapped.

Aneurysm wall has discrete phase reflection coefficient set to 1 perfect reflection, and stent wall uses the trap boundary condition to count the number of particles that reach the boundary surface.

Regarding MHD aneurysm wall acts as isolating wall, since there is no electric current going through the boundary. Stent wall acts as a thin wall that has a finite electrical conductivity.

- **Outlet BC**

The outlet pressure is chosen as a reference pressure, which is defined a constant pressure of 0 Pa. Outlet surface is defined as escape boundary condition for the discrete phase model.

Boundary conditions are summarized in Figure 5-4

Figure 5-4. Boundary Conditions summary

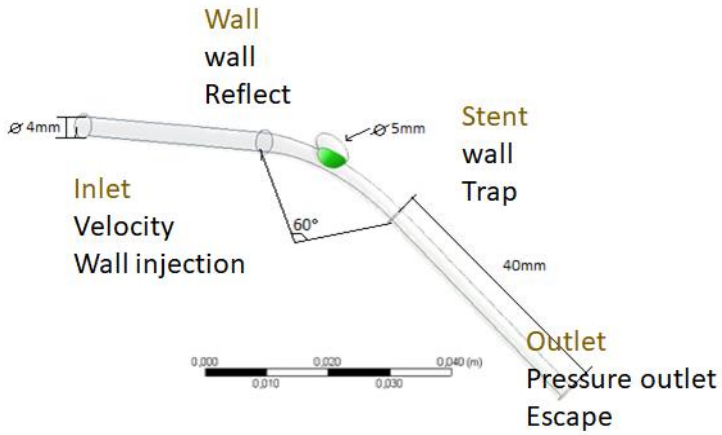

5.2.4 Numerical approach

The flow model can be well described with Navier-Stokes equations, Newton's second law of motion and Maxwell's relations which explain the fluid flow and particles motion.

The discrete phase model is implemented with a Lagrangian approach. Blood, as the fluid phase, is treated as a continuum by solving the Navier-Stokes and Maxwell equations, following the same approach described previously in 5.1.4.

The motion of cells is dominated by the magnetic Lorentz force, fluid drag force and Shaffman lift force. Inertia force, gravitational force and buoyancy force are neglected due to their small magnitude compared to dominant forces listed above.
Other factors such as cell–particle and particle–particle interaction forces are not considered either.

The trajectory calculations are based on the force balance on the particle, using the local continuous phase conditions as the particle moves through the flow. The particle trajectory is computed through the equation of the balance of forces acting on that particle.
After each iteration for each particle, the information about position, time, and three components of velocity as well as the speed with which the particles cross the control volume boundaries are obtained. In a steady simulation, the dose of cells is injected into the artery and the trajectories are described by governing equation (4-13)

ANSYS Fluent 16.1 [149] simulation is used for processing with a pressure-velocity coupling, using the SIMPLEC segregated solution algorithm. To appraise the magnetic field amplitude, frequency and direction required to attract and maintain endothelial cells in the stent, coupled DPM, is performed. In accordance with Ghosh thesis [158], where magnetic microparticles have been injected in a steady state manner, in this approach particles are included only in the postprocessing to calculate and display particle tracks.

- **Steady blood flow**

The flow in the channel is treated as laminar, non-Newtonian, incompressible, fully developed and steady. It is solved using the Navier–Stokes and Maxwell equations coupled.
Considering the numerical settings presented in Table 5-2, the mesh independency analysis is performed.

Table 5-2 - Spatial Discretization

Pressure-Velocity Coupling	Spatial Discretization			Convergence Criteria
	Gradient	Pressure	Momentum	
SIMPLEC	Least Squares Cell Based	2ndOrder	2ndOrder	$1x10^{-5}$ (in all residuals)

For steady flow, it is possible to define steady or transient tracking of the particles. For steady analysis, as soon as the particles are released, they are tracked until they reach the destination according to the specified boundary behavior.

5.2.5 Mesh-independent analysis

The mesh elements used in the work are tetrahedral with a minimum element quality of 0.26 skewness for the whole domain. Finer meshes are applied in the stent and other regions close to the stent.

Three different meshes are created and WSS is calculated in the middle point of Stent wall, as presented in Table 5-3. Differences within 5% are observed for the WSS in the stent region. Thus, this mesh setup can guarantee the correctness of the simulation results. In addition, WSS along the ostium line is presented in Figure 5-5 for the meshes. It can be seen mesh 2 and 3 have minimal difference between them along the line.

Table 5-3 Mesh-independent analysis

	Number of elements	Max Skewness	WSS point in the middle of Stent wall [Pa]	% difference successive mesh densities
Mesh 1	114812	0,87092	30	
Mesh 2	2139088	0,84609	22	30%
Mesh 3	2646129	0,84002	21	5%

Figure 5-5 WSS along ostium line

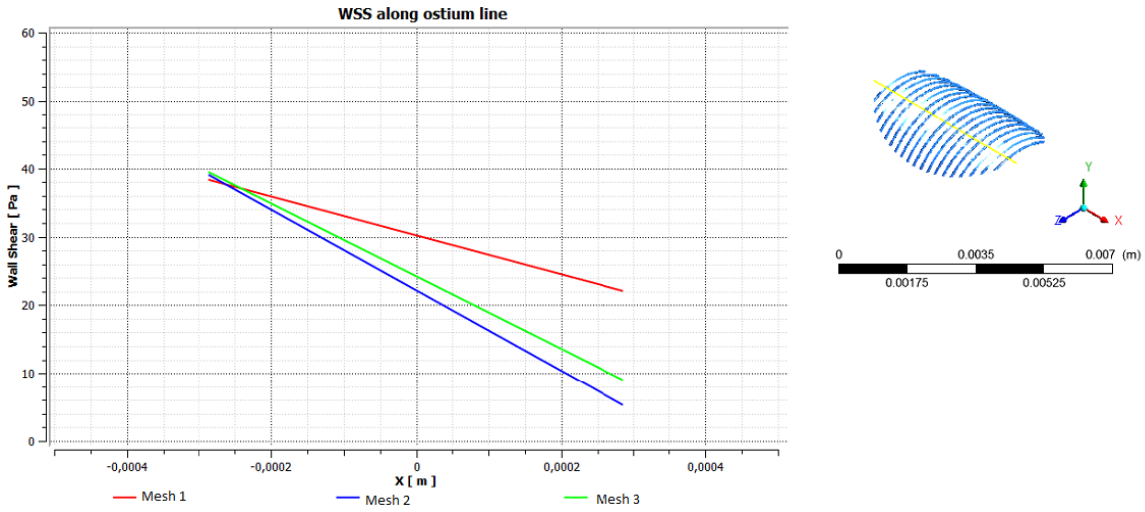

Figure 5-6 shows the final mesh resolution

Figure 5-6 – Stented Mesh- Final mesh resolution. a. partition for mesh creation b.XY clip c. YZ clip

a. b. c.

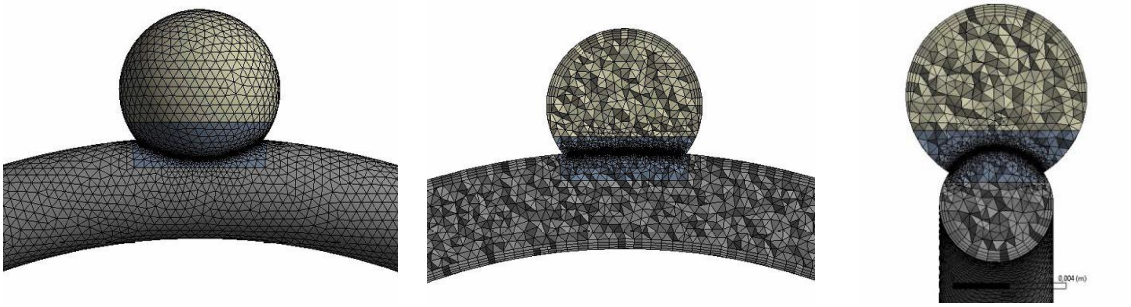

5.2.6 Statistical analysis

To study the combined effect of the magnetic field factors over the capture efficiency, a statistical analysis is performed.

It is established as a null hypothesis that If the amplitude, frequency and direction of the magnetic field applied to the region of interest changed, then there is not significant difference in the cells capture efficiency on the stent region.

A design of experiments (DOE) factorial design 2^3 is proposed. Statistical significance is determined via one-way ANOVA with Statistical Software Minitab 17.0 [159]. The independent variable to be study is the capture efficiency in the stent region. Using the number of trap particles and Eq. (3-1), the capture efficiency is calculated. Statistical significance is defined as a probability value of $p<0.05$.
The one-way ANOVA compares the means between the factors and determines whether any of those means are statistically significantly different from each other.

According with the specific aims, the 3 considered factors for the DOE are: magnetic field amplitude, frequency and direction. As presented in Table 5-4, each factor has a low and high-level according with the physical possibilities previously discussed in 3.2, to be consistent with the cells capture analysis. Since the response variable is studied using computational analysis, repetitions of the experiment are not considered in the DOE. Principal effects and the combined effects are studied.

Table 5-4 – Considered factors for the Statistical analysis with the corresponding low and high-level

	Amplitude	**Direction**	**Frequency**
High Level (1)	1 T	Y - Open bore	AC= Electromagnetic
Low Level (-1)	0.5 T	(-Z) - Closed bore	DC = Permanent magnet

Table 5-5. ANOVA experiment distribution

	Random run	**Amplitude**	**Direction**	**Frequency**	**Headline of the model**
1	4	1	1	-1	1T – Y – DC
2	6	1	-1	-1	1T – (-Z) – DC
3	3	-1	1	-1	0.5T – Y – DC
4	2	-1	-1	-1	0.5T – (-Z) – DC
5	8	1	1	1	1T – Y – AC
6	1	1	-1	1	1T – (-Z) – AC
7	7	-1	1	1	0.5T – Y – AC
8	5	-1	-1	1	0.5T – (-Z) – AC

.

6. Results and Discussion

6.1 Results: Hemodynamic changes on a wide-neck aneurysm under the presence of a uniform magnetic field

Velocity contours at different magnetic field B= 0, 0.5 and 1 T are plotted at systole peak in the third pulse (t=2,18s) using XY and YZ planes. Figure 6-1(a-d) shows velocity contours at the center plane XY, Z=0 and (e-h) the results in the cross-section area at plane YZ, X=0 using the same scale.

Average velocity of the blood flow in the neck and inside the sac is reported in Table 6-1.

Table 6-1. Average velocity in neck and sac

	(a)without Magnetism	(b) 0.5 T	(c) 1 T
Average Velocity in the neck	0,52 m/s	0,66 m/s	0,71 m/s
Average Velocity inside the sac	0,04 m/s	0,32 m/s	0,55 m/s

As presented in Figure 6-1, aneurysm geometries are isolated from their parent arteries and data analysis is presented by two cut planes positioned at the ostium. The external magnetic field change the direction of velocity field where the blood flow is pushed strongly in the direction of the magnetic field, making possible to accumulate blood in the aneurysm neck where the tunica media is missing. In addition, it is shown that the velocity magnitude decreases when the intensity of the magnetic field increases, creating vortexes that help to staunch the ferrofluid flow.

Figure 6-1: Velocity contours at different magnetic fields, center plane (a-c) and cross-section area (d-f)

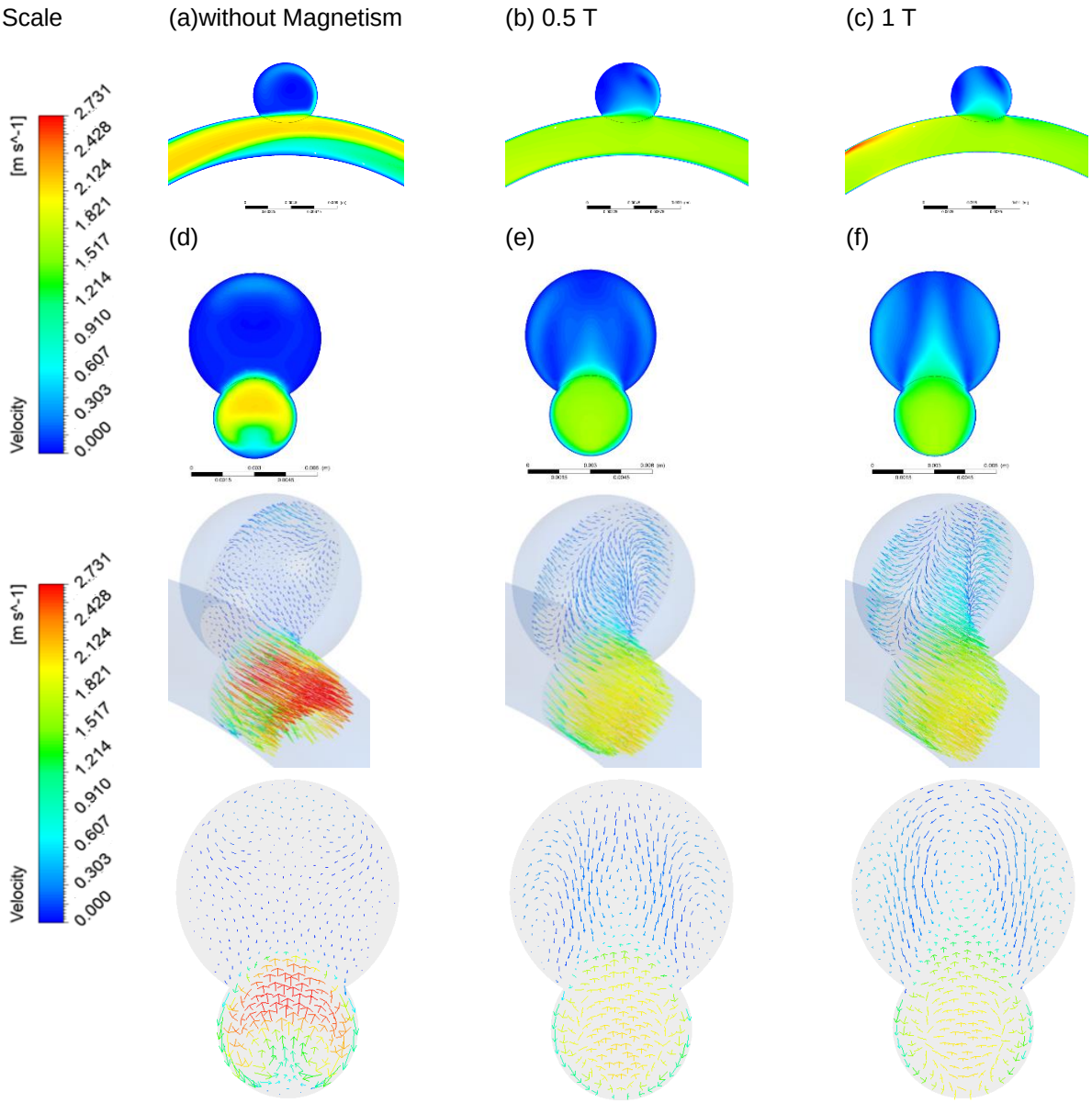

Figure 6-2 presents the points of analysis where WSS and pressure are calculated.

Figure 6-2: Points of interest in the saccular aneurysm analysis.

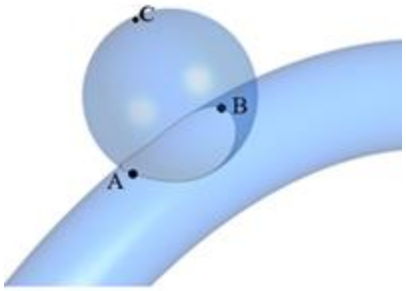

As presented in Figure 6-3(a-b) point A neck inlet, a large magnetic field promote an increase on the temporal variation of WSS in the pulsatile environment of the non-Newtonian behavior. The effect is most notable in the systolic phase, although the curves have a slightly different behavior.

This increment is explained by the abrupt change of velocity that occurs at the distal neck region (point A), where the inflow impacts. The pressure at this point is not extensively affected.

Figure 6-3: Temporal evolution of WSS at three characteristic points (neck Inlet – outlet and bulge top) for different magnetic field magnitudes

(a) WSS [Pa] vs t[s] point A neck inlet

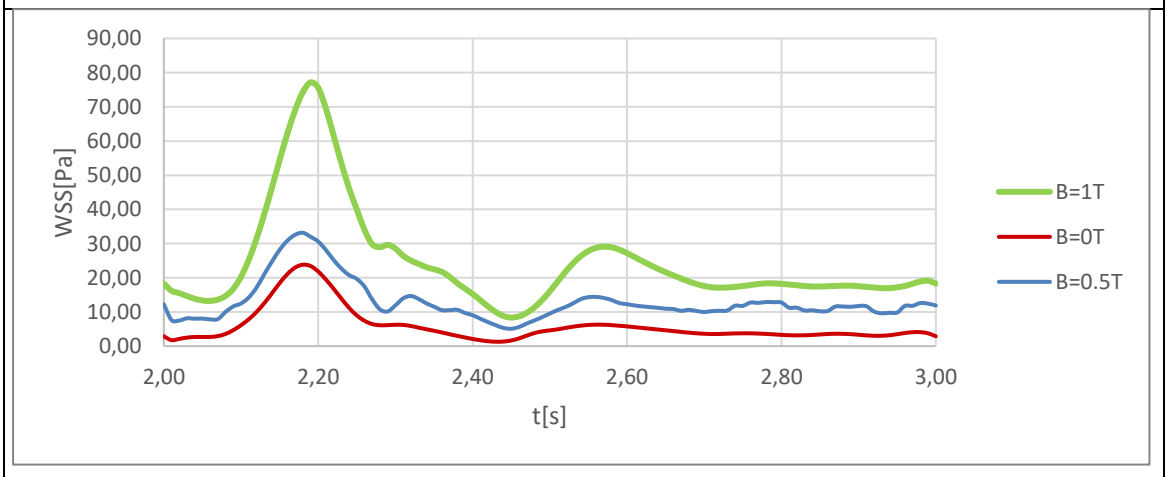

(b) P [Pa] vs t[s] point A neck inlet

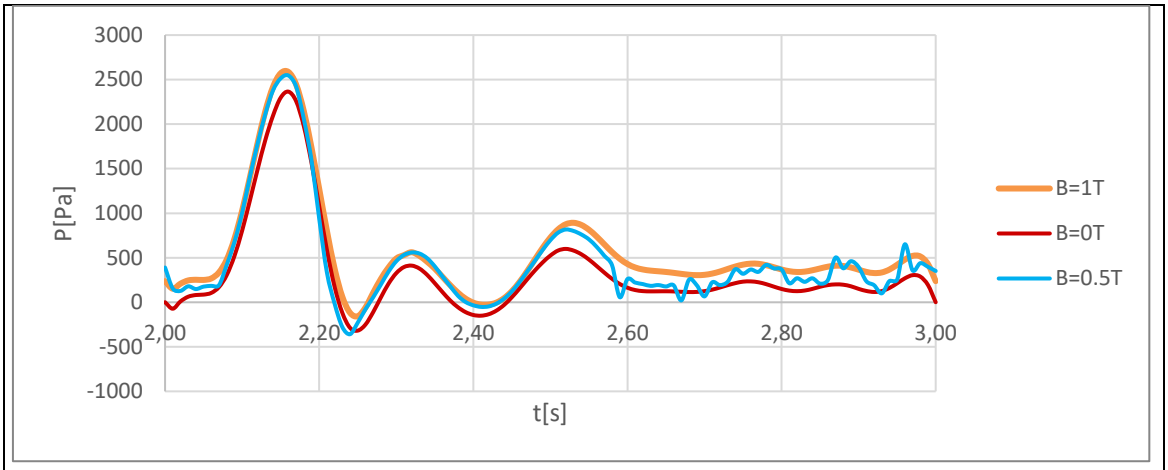

(c) WSS [Pa] vs t[s] point B neck outlet

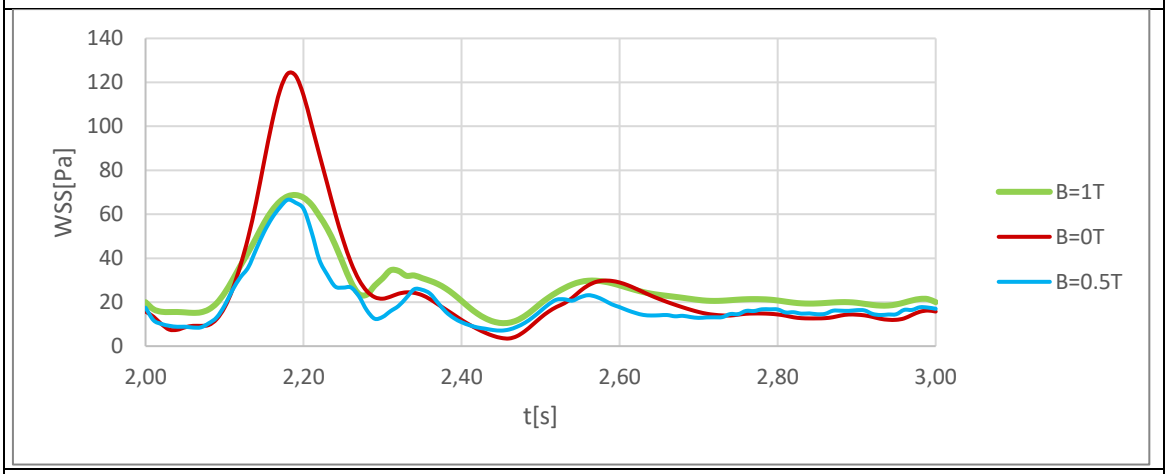

(d) P [Pa] vs t[s] point B neck outlet

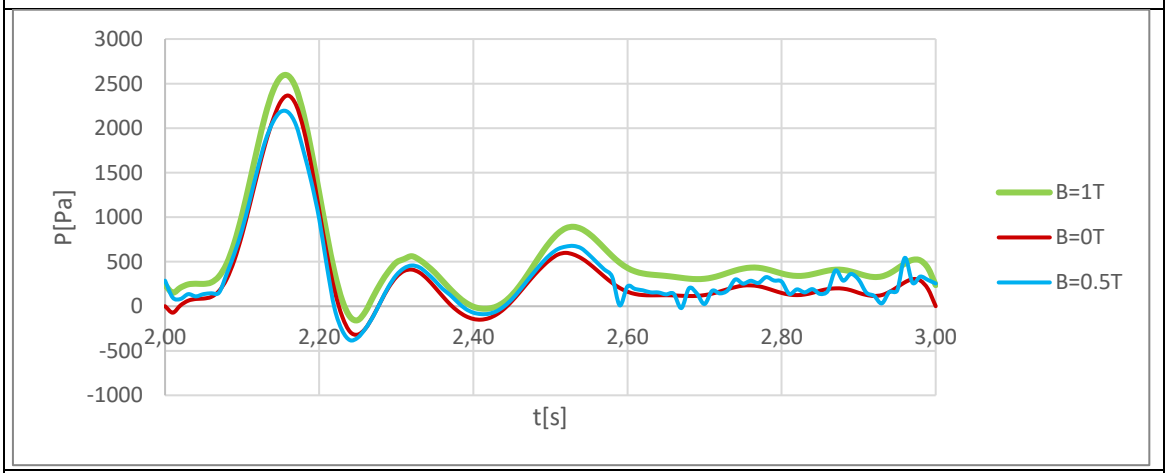

(e) WSS [Pa] vs t[s] point C bulge Top

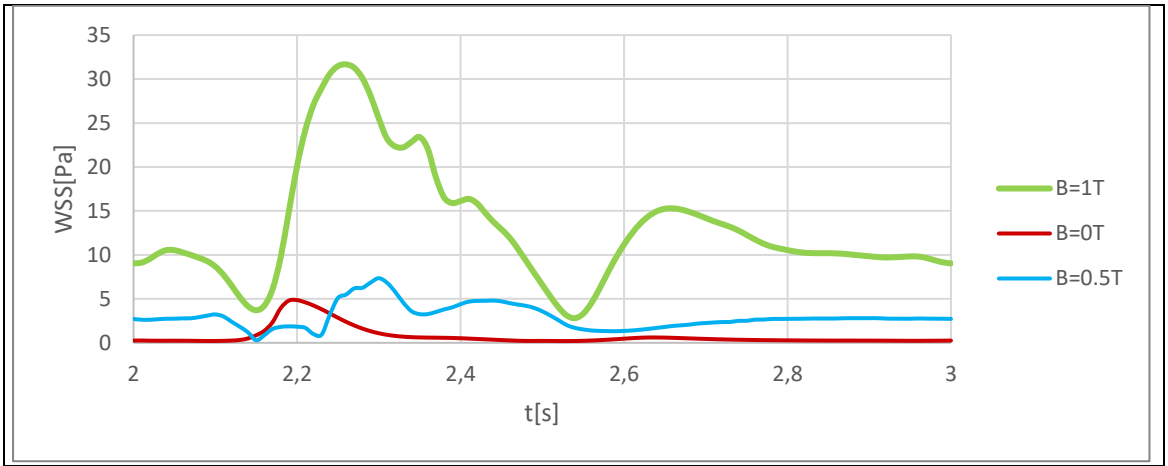

(f) Pa [Pa] vs t[s] point C bulge Top

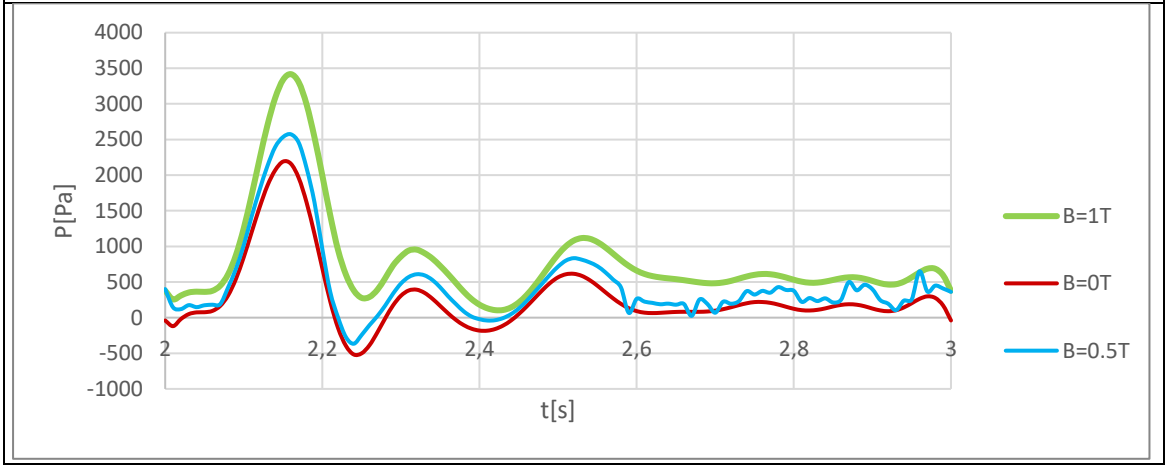

As presented in Figure 6-3, results at systole phase (0,18 s) show that under the action of an applied external uniform magnetic field the temporal variation of WSS increases in the neck of the aneurysm at the inlet of the blood flow, point A and for the bulge top, point C. At the top of the sac it is also shown that pressure and WSS grows significantly. Finally, for the point B neck outlet WSS is reduced.

6.1.1 Discussion

The use of idealized geometric models are a crucial strategy to study multiphysic phenomenon since it allows to isolate the effect of geometry on the overall hemodynamics analysis [86]. The idealized model of blood flow inside a non-treated aneurysm, reported

by Xu *et al* [129] is used to qualitatively compare the flow pattern of the model without magnetism presented in the current thesis.

Both models have considered 60º in the parent vessels curvature and pulsatile inlet velocity. Despite Xu *et al*, simulated the blood flow as Newtonian fluid, while the current work considered non-Newtonian behavior none discrepancies are observed between the reported inflow velocity by Xu *et al* and the gotten flow pattern.

Average velocity values reported in Table 6-1 for the simulation without magnetism are numerically compared with corresponding values for an unstented idealized model reported by Lopez Ramirez [58] in his thesis. Values are in the same order of magnitude. As expected, by comparing the average velocities among the simulations, the model without magnetism shows a smaller spot of blood moving at less velocity inside the aneurysm.

From the idealized simulation results described above, it is shown that a localized magnetic field considerably influences the blood flow, the flow outside the sac is deflected and slowed down in proximity the magnetic location. Velocity reduction have been previously identified by different authors [87], [154], [160]. The phenomenon can be explained due to electromagnetic induction. When a magnetic field is applied over a moving electrically conducting fluid, electrical currents are induced in the fluid. The interaction between induced currents and magnetic field produces Lorentz forces as an external force that acts as a resistive drag force that decelerates blood flow.

Streamwise velocity decreases and the Pressure and WSS grows significantly at the top of the sac. This behavior can be explained considering that the magnetic field has virtually pushed more blood to the sac, causing a strong deflection and simultaneously, increasing the pressure.

Under the action of the applied external uniform magnetic field, the velocity of the blood flow decreases and its direction is redirected to the bulge creating a stagnant fluid at the aneurysm neck. This occurrence provides an appropriate condition for EC recruitment on

a specific location, since the residence time of the blood, as carrier fluid, increases simultaneously particle deposition [17], [95].

In addition to blood velocity, WSS plays a crucial role in reendothelization [59]. Increment in the pulsatile WSS and Pressure at the inlet of neck, where blood flow enters to the sac, is desirable. As presented by [46], it promotes the cells attachment. Meanwhile the reduction of the WSS on the other end of the neck would help the cells to align parallel to the blood flow according with [20].

The presented CFD model gives relevant elements that allow to predict the behavior of biomagnetic fluid flow in the presence of the magnetic field and to understand the effect of applying a uniform external magnetic field for cells recruitment. Further realistic models are suggested to consider the effect of the pulsatile environment on the wall vessels and its effect on the disturbed blood flow.

6.2 Results: Influence of magnetic configuration on magnetic cells targeting efficacy

Before studying the effects of different configuration of magnetic field on the particle capture efficiency, virtual stent is positioned in the saccular brain aneurysm and hemodynamics changes are evaluated. Blood flow direction used for the results is presented in Figure 6-4.

Figure 6-4 – Velocity direction of blood flow. The blood flow direction is from left to right.

a.

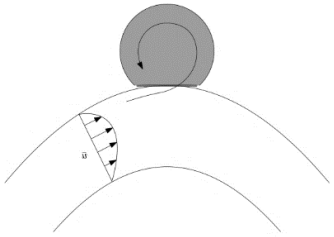

Differences in the velocity field related with the presence of virtual stent are presented using the velocity contours in Table 6-2 in the two middle planes of the model. It can be appreciated that virtual stenting reduces the velocity field inside the sac by 61%.

The main aim of this section is to investigate the particle transport and capture efficiency when blood flow is submitted to different magnetic field conditions.

After the virtual stenting validation, the stented model is used to calculate the hemodynamic under different magnetic fields. First, the continuous phase flow field is calculated and velocity field and WSS is analyzed, then, particle trajectories and fate for discrete phase injections are determined.

Table 6-2. a. Velocity field in virtual Stented model without magnetic field displayed in plane XY. b. Velocity field in virtual Stented model without magnetic field displayed in plane YZ. c. Velocity field without stent - No magnetic field displayed in plane XY. d. Velocity field without stent - No magnetic field displayed in plane YZ

Velocity field in virtual Stented model– No magnetic field	
a. 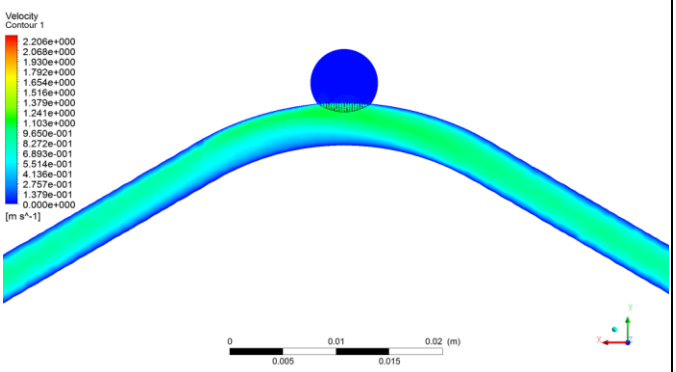	b. 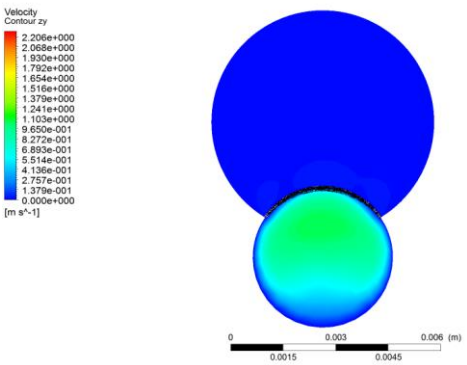
Velocity field without stent - No magnetic field	
c. 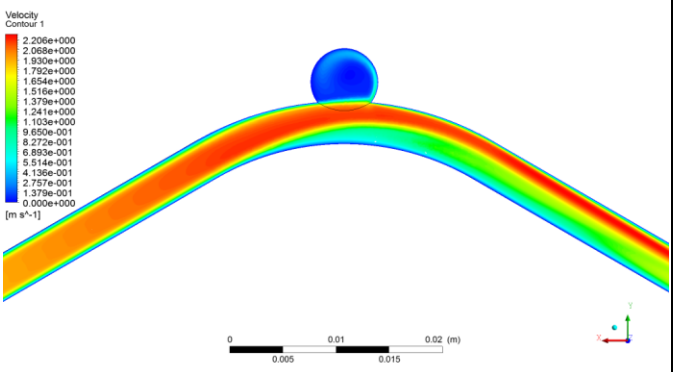	d. 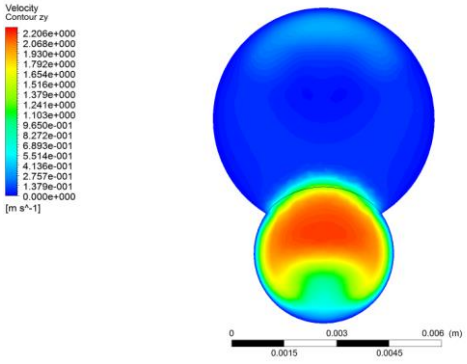

- **Continuous phase flow field**

8 simulations are performed combining the factors described in Table 5-4, high and low levels considered in the simulations are: 1T and 0.5 T for the amplitude. Direction is varied according with the MR scanner configuration, 90º in -Z for cylindrical configuration and 90º in Y for open bore MRI configuration. Finally, frequency is varied between electromagnetic (AC) and permanent magnet (DC).

Using the same report planes presented in Table 6-2 for the reference non-magnetic model, Table 6-3 presents the velocity field contours in mid plane XY and YZ along the domain of interest for the simulations with magnetic field applied. The maximum velocity value is presented above for each corresponding model. The headline of each model indicates the Amplitude – Direction – Frequency.

Table 6-3. Velocity field in the domain of interest

Models	Velocity field Plane XY	Velocity field Plane YZ
1T – Y – DC	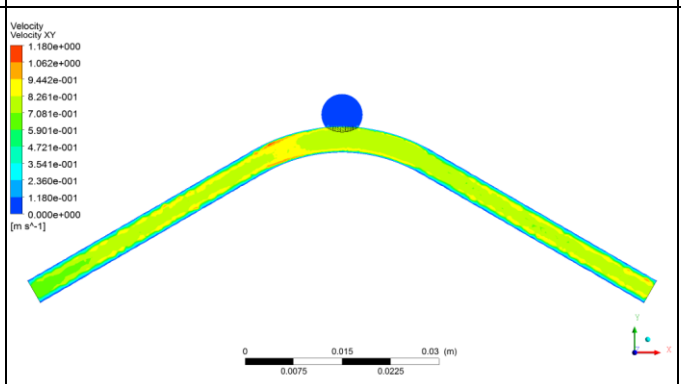	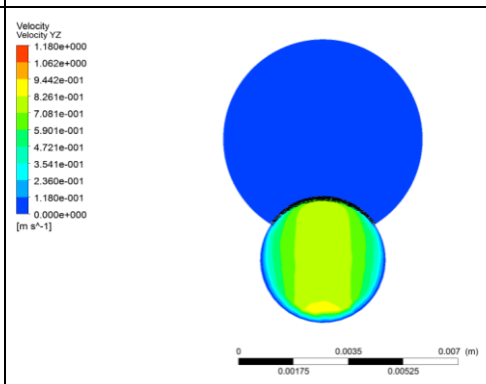
1T – (-Z) – DC	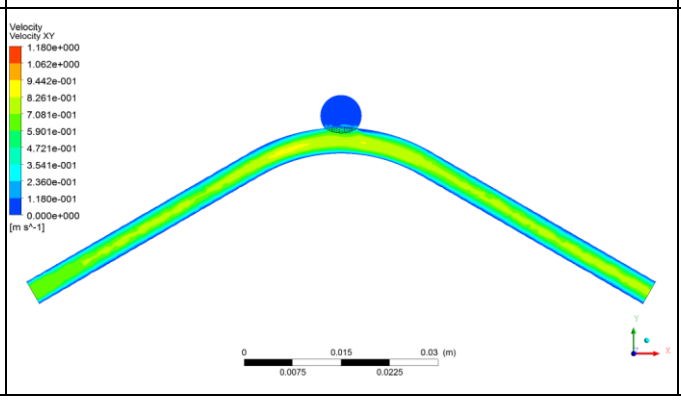	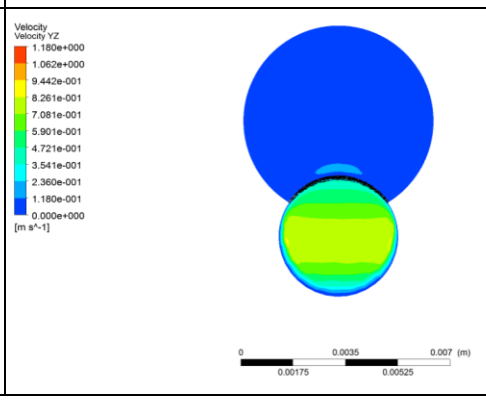

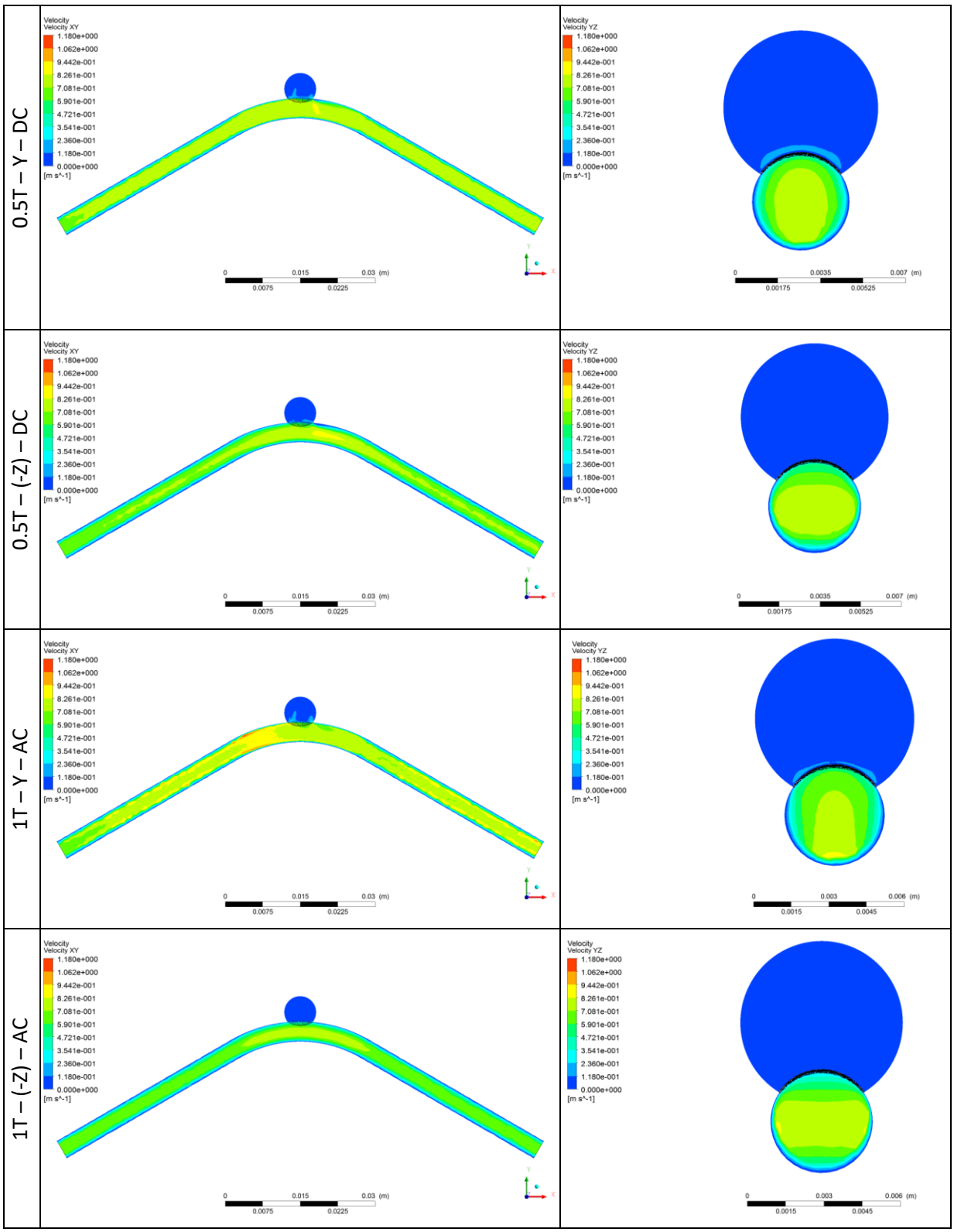
0.5T – Y – DC
0.5T – (-Z) – DC
1T – Y – AC
1T – (-Z) – AC
Velocity
Velocity XY
Velocity YZ
1.180e+000
1.062e+000
9.442e-001
8.261e-001
7.081e-001
5.901e-001
4.721e-001
3.541e-001
2.360e-001
1.180e-001
0.000e+000
[m s^-1]
0
0.015
0.03 (m)
0.0075
0.0225
0.0035
0.007 (m)
0.00175
0.00525
0.003
0.006 (m)
0.0015
0.0045

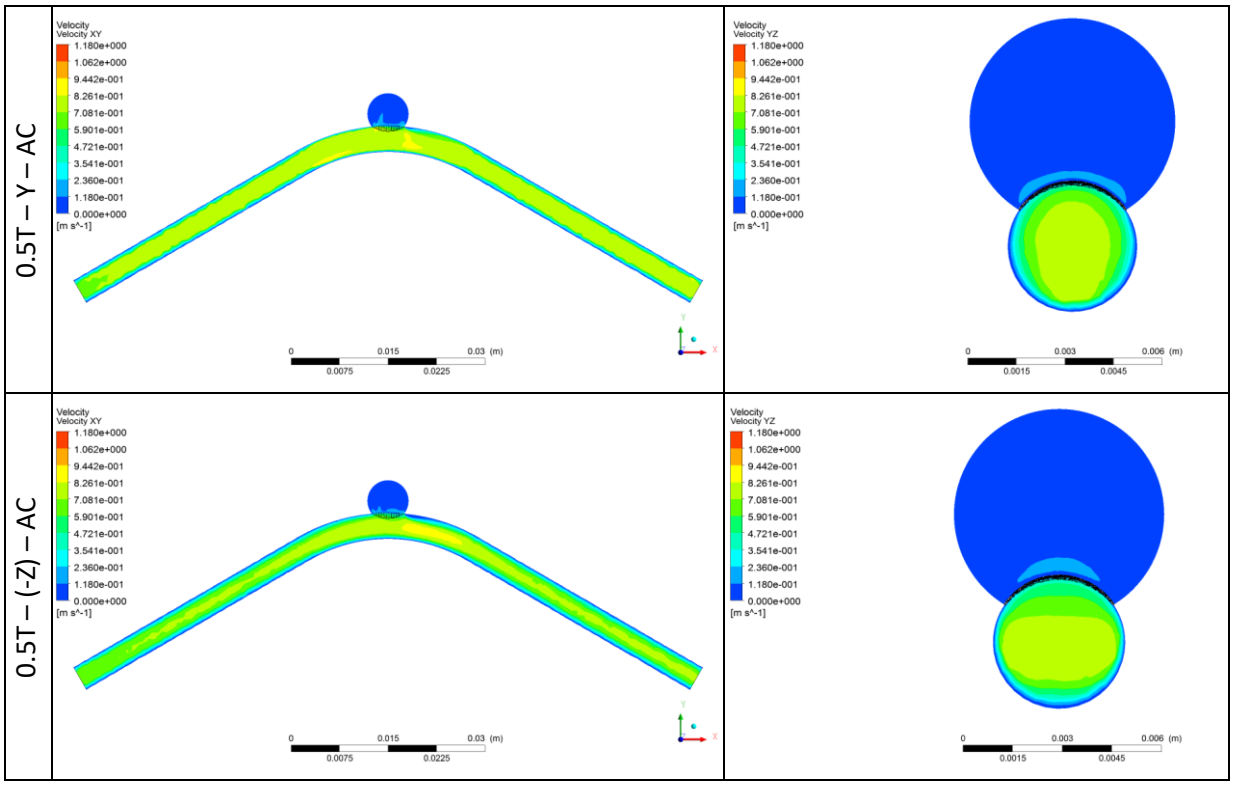

It can be identified that different magnetic configuration affects blood flow pattern, which is most noticeable in YZ plane. For the same amplitude and frequency, a change in the magnetic field direction, encourages a change in velocity field distribution in all the cases. There is a flow separation downstream the sac, at the outlet of the neck, that can be seen in XY plane. It is more prominent when magnetic field is applied in (-z) direction, that represents a greater impact of magnetic field in a cylindrical MRI machine, compared to open bore direction. For the same direction and frequency, it can be seen that greater amplitude decreases the blood flow velocity downstream the sac. It has not been identified a clear variation in blood flow velocity contours, when only frequency is changed.

The most interesting region to analyze the influence of magnetic configuration on magnetic cells targeting efficacy is the ostium, where the stent is located. Figure 6-5 shows the middle line in the ostium, velocity across this line is calculated for each model and compared in Figure 6-6.

Figure 6-5. Ostium line

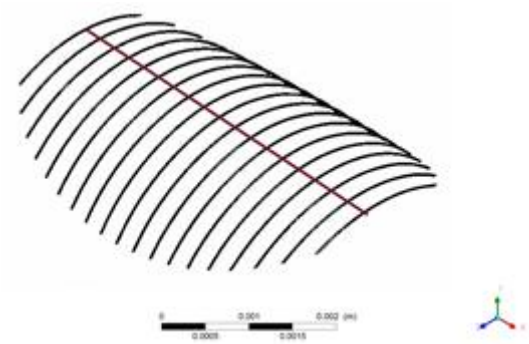

Figure 6-6. Velocity comparison in Ostium line

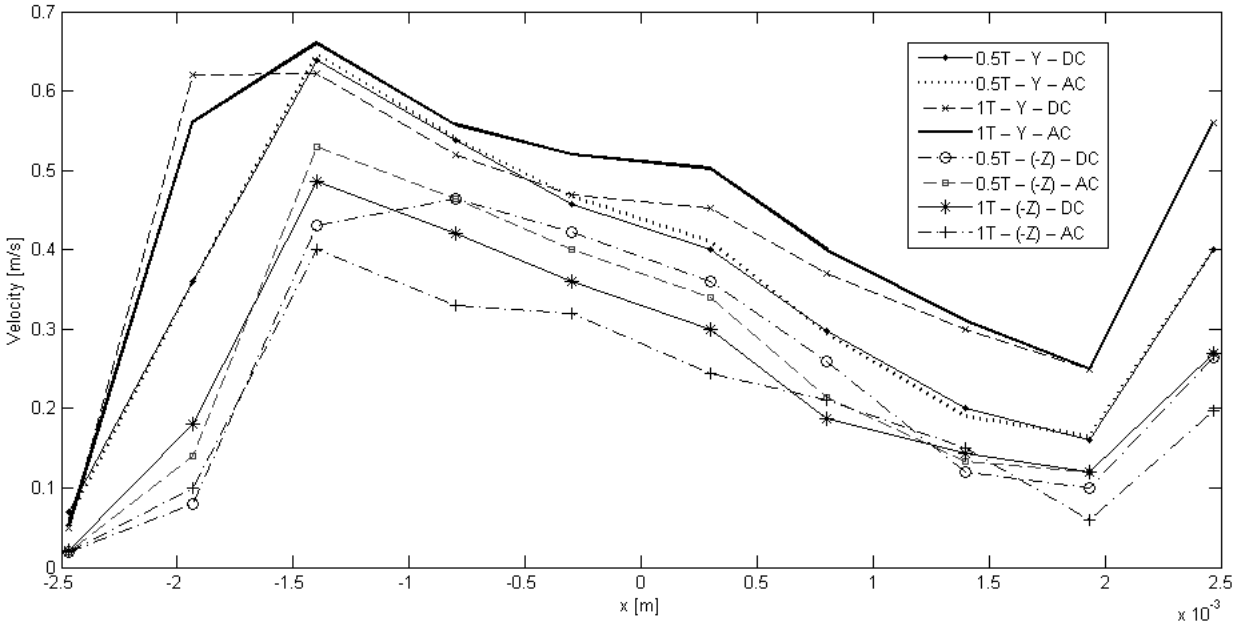

In addition to the velocity analysis, WSS in stent wall is calculated for each model and presented in Table 6-4. Comparison with non-magnetic model is done.

Table 6-4. WSS in the stent wall for each model

Models	WSS	WSS Bottom view
Non Magnetic model	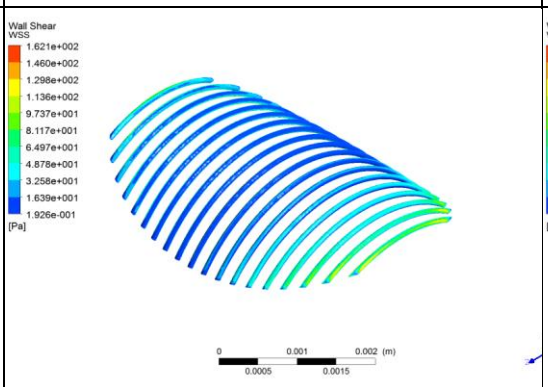	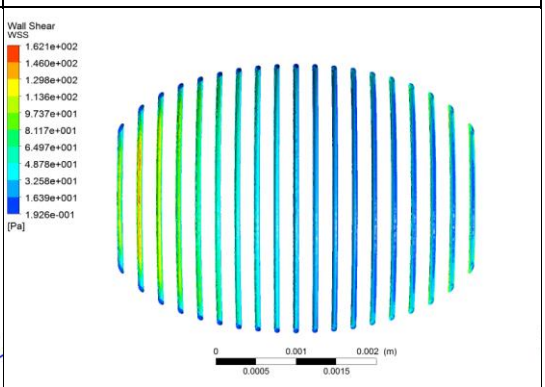
1T – Y – DC	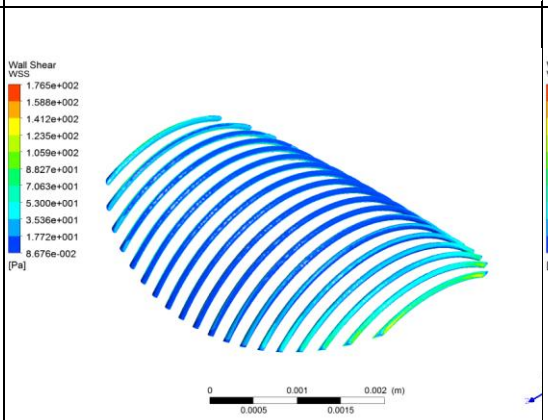	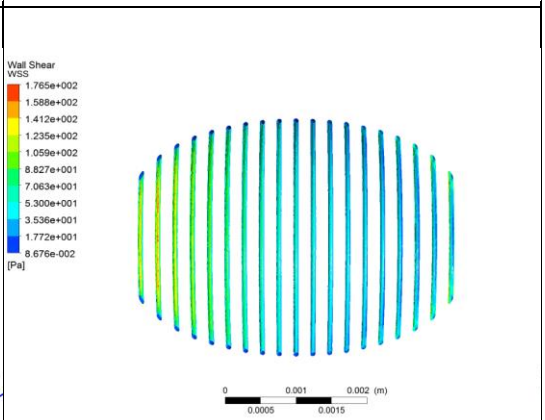
1T – (-Z) – AC	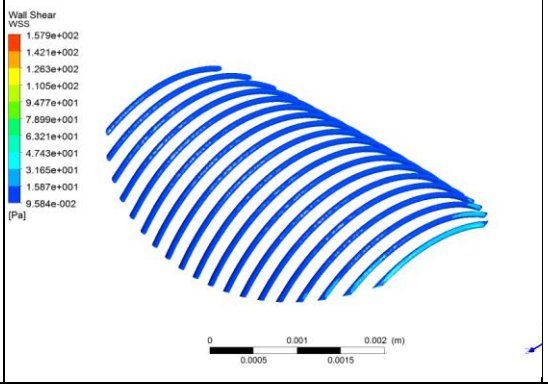	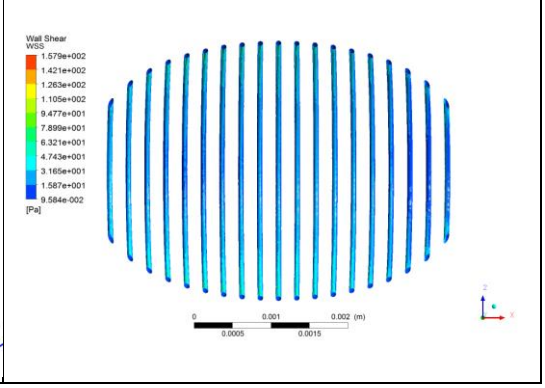

0.5T – Y – DC	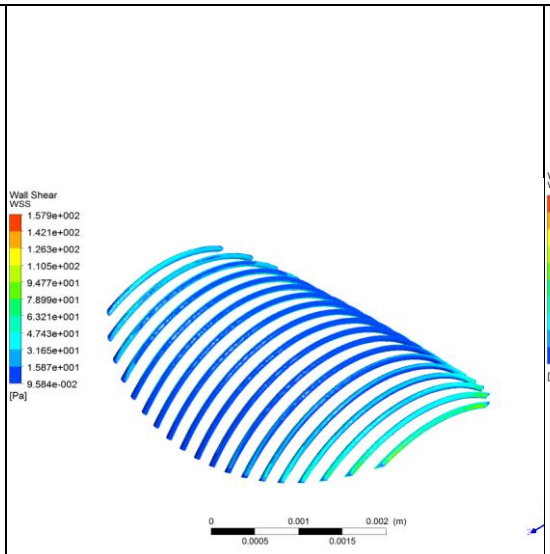	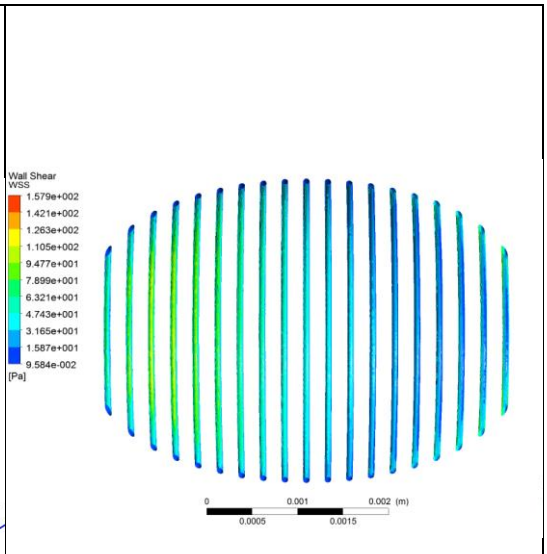
1T – (-Z) – DC	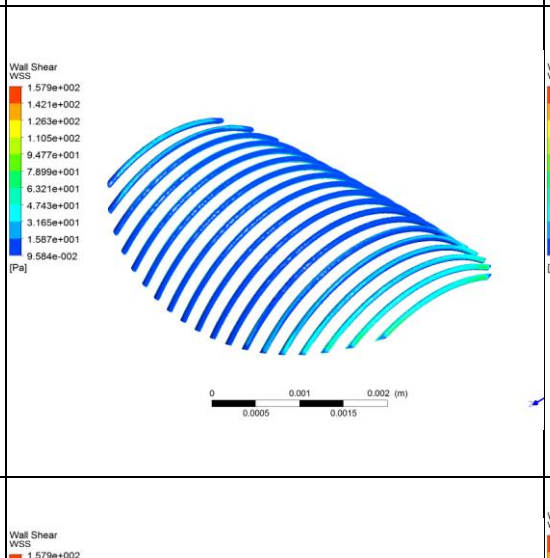	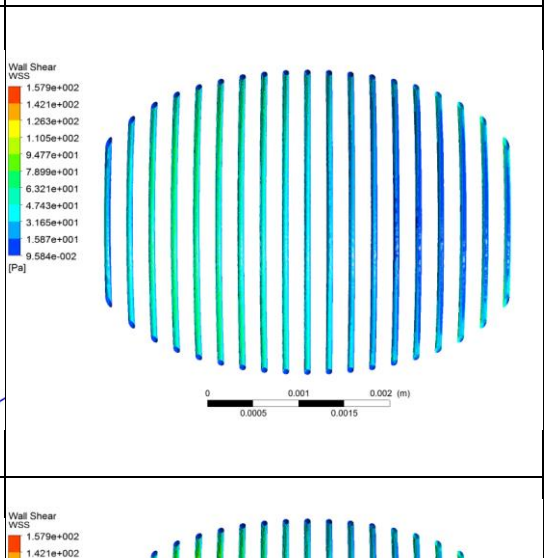
1T – Y – AC	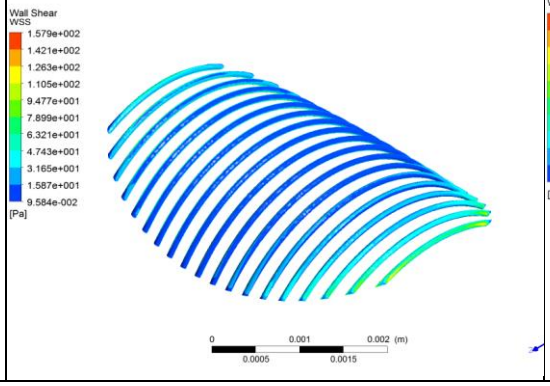	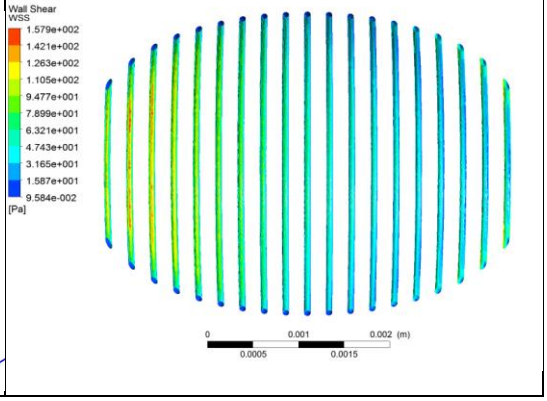

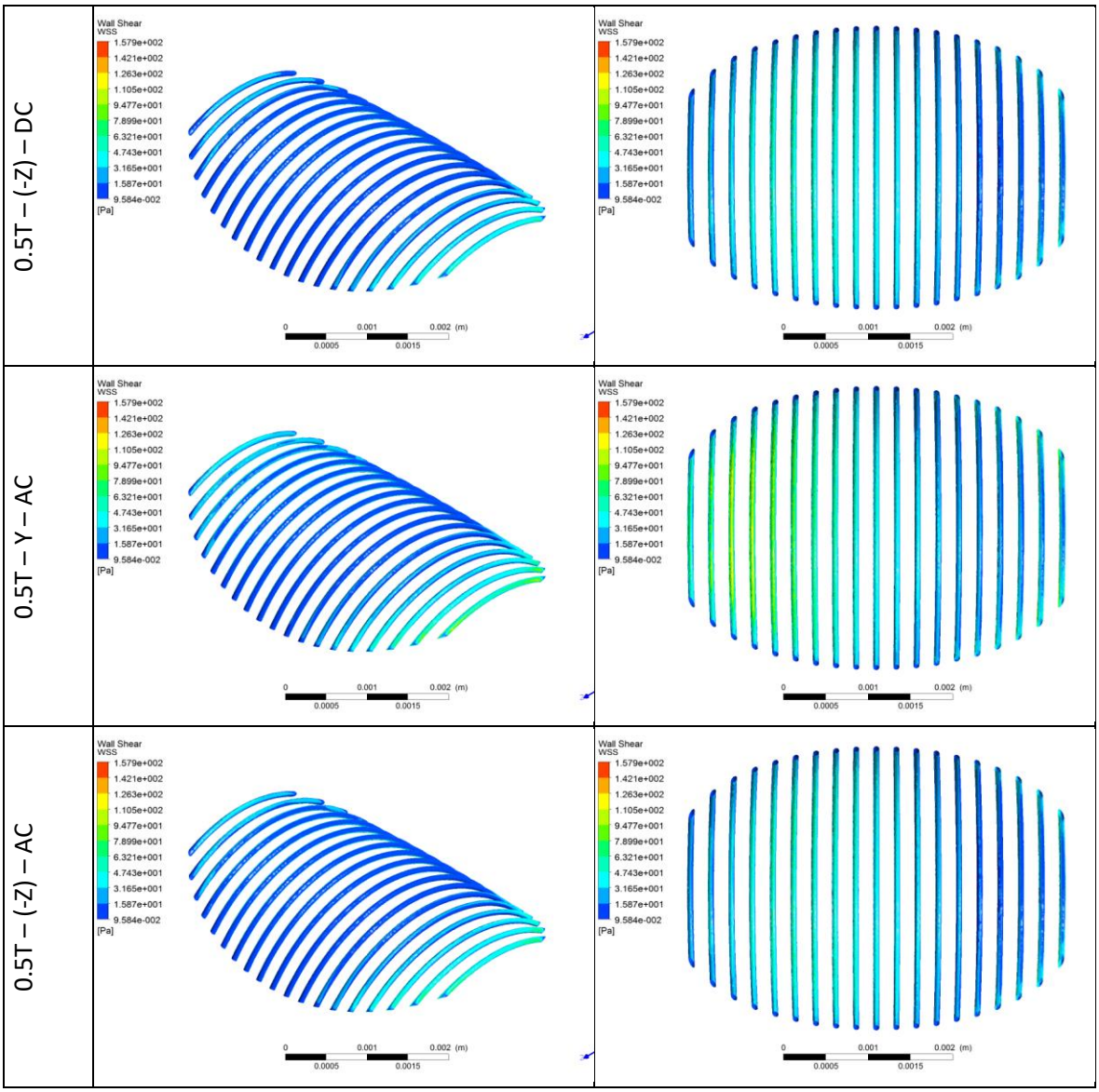

Low WSS values are observed within the stented region of all simulations. From the bottom view it can be identified that WSS is greatest in the middle of each stent strut independent of strut length. It is in concordance with the flow direction entering the aneurysm sac after bumping into the stent. In addition, it can be observed that proximal region has the greatest WSS value for all the models.

After magnetic field application WSS decrease the maximum value for almost all the models. Only the model for permanent 1T magnet in Y direction (open bore MRI) has a greater WSS value (176 Pa) when comparing with non-magnetic model (162 Pa).

- **Particle capture efficiency**

After the injection of the total number of particles to be tracked, DPM Particle fate is recorded and summarized as a particle history file. If particles pass over the magnet, and goes downstream in the negative Y-direction, the particles miss the target and escape from the outlet boundary. Particles whose trajectory is interrupted by the stent wall are considered trap.

It is considered a satisfactory simulation of the discrete phase when 95% of the particles have a define fate at the end of the DPM iterations.

Table 6-5 presents the number of trapped particles in each model, with the correspondence capture efficiency calculated from equation (3-1). The results assume the injection of 14.520 identical non-interacting magnetic particles in the carrier fluid, all of them are completely saturated. Results presented in this table are further used for the statistical analysis.

Table 6-5. Number of trapped particles and capture efficiency.

	Amplitude	Direction	Frequency	Models Description	# of Trapped particles	Capture Efficiency
1	1	1	-1	1T – Y – DC	12.696	87,438%
2	1	-1	-1	1T – (-Z) – DC	5.383	37,073%
3	-1	1	-1	0.5T – Y – DC	10.187	70,158%
4	-1	-1	-1	0.5T – (-Z) – DC	3.848	26,501%
5	1	1	1	1T – Y – AC	11.097	76,426%
6	1	-1	1	1T – (-Z) – AC	1.409	9,704%
7	-1	1	1	0.5T – Y – AC	10.828	74,573%
8	-1	-1	1	0.5T – (-Z) – AC	688	4,738%

It can be noticed from Table 6-5 that biggest target efficiency is obtained for the configuration 1T in an open bore MRI scanner with permanent magnet and smallest capture efficiency is get on a cylindrical MRI scanner with the 0.5T magnetic field amplitude, when the domain is under an electromagnetic magnet.

Comparison with non-magnetic field model is done, where only one particle was trapped, corresponding to 0,007% capture efficiency.

In order to identify if the factors have an statistical incidence over the number of trap cells, the DOE results are presented in Table 6-6 the graphics are obtained using Minitab [159]. With an α of 0.05, the p-value (0.001) in the Analysis of Variance table provides enough evidence to conclude that the direction of magnetic field has incidence statistically significant for the capture efficiency.

Table 6-6 – Statistical results ANOVA study. From Minitab 17.0 [159]

Source	DF	Adj SS	Adj MS	F-value	P-value
Amplitude	1	0,01503	0,01503	2,04	0,227
Direction	1	0,66458	0,66458	90,08	0,001
Frequency	1	0,03882	0,03882	5,26	0,084
Error	4	0,02951	0,00738		
Total	7	0,74794			

Analysis of variance Capture Efficiency Model summary
S = 0,0858958 R-cuad. = 96,05% R-cuad.(Adj) = 93,09%

Four-in-one residual plot from Figure 6-7 is used to verify statistical assumptions. Normal probability plot follows a straight line indicating that the residuals are normally distributed. Due to the lack of replica, histogram does not show a normal behavior. In addition, residuals are randomly distributed around zero in versus fit plot and residuals display no obvious pattern, this suggests that there is not time dependence of the residuals.

From Figure 6-8 it can be identified that direction has greatest incidence on the capture efficiency.

Figure 6-7. Four-in-one residual plot. From Minitab [159].

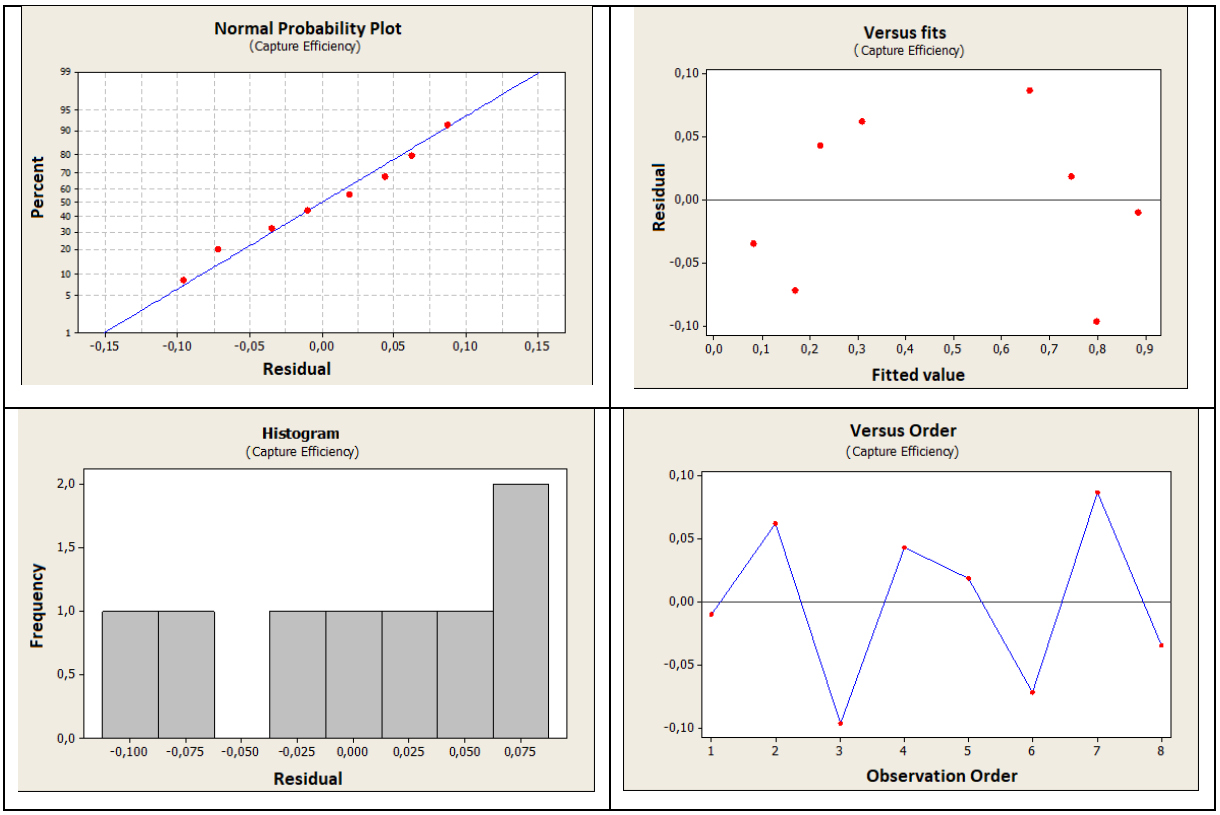

Figure 6-8. Pareto Chart of the effects

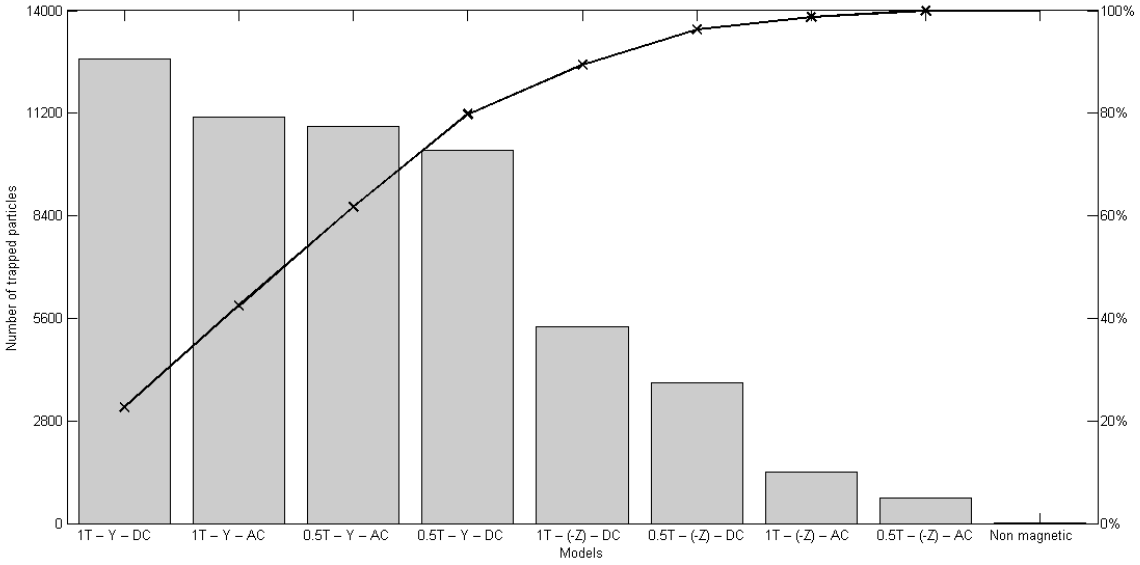

6.2.1 Discussion

Previously, some authors have demonstrated the benefits of delivering cells to enable rapid endothelialization of vessels [14], [18], [40], [53]. Effects of magnetic field, particle size and flow velocity on the capture efficiency of magnetic particles have been previously reported. However, in the current state of bibliographical revision, it has not been successfully encountered controlled experiments with well-characterized flow conditions that study the incidence of different magnetic physical features on the capture efficiency of superparamagnetic labeled cells on saccular brain treated aneurysm. As part of the main aim of the project, it is important to appraise the magnetic field configuration required to attract and maintain endothelial cells to the stent wall. According with [16], in order to provide a uniform magnetic field in the region of a deployed stent, in a clinical configuration two different configurations can be evaluated, a regional application of large permanent magnets, or carrying out the targeting procedures in an MRI device. It represents two different magnetic field frequency alternatives. In addition, Connell *et al* [15] introduce that not only the amplitude is enough to attract the particles in the flow, adding the amplitude as a second variable to be considered in the particle capture efficiency. To contemplate typical MRI system with a uniform magnetic field in the 0.5- to 1 Tesla range, open and cylindrical configurations should be studied, it implies differences in the magnetic field direction. Computational results reported in this work help to improve the fundamental understanding of the hemodynamics changes in treated aneurysm under all the clinical configuration that currently generates external magnetic field. In addition, results promote the hemodynamics-based predictions of treatment outcomes from novel treatment strategies, that could impact patient outcomes.

Flow diverter stent incidence in blood velocity and stent wall shear stress is studied. It is found that there is influence of stent position on blood velocity magnitude inside the aneurysm sac. The differences found in treated vs non treated aneurysm reflects the same results previously presented by different authors [58], [118], [161], where separation at the leading edge and recirculation inside the aneurysmal sac occur. In addition, a single recirculating vortex is found inside the aneurysm in the ostium region. Results are acceptable, and model is validated to proceed to include the magnetism effect.

In the magnetic blood flow simulation, similar to Sharma *et al* [80] results, it can be noticed by velocity contours that the presence of a magnetic force causes the decrease in axial flow velocity of blood appreciably. Since Sharma study is performed in a cylindrical tube with magnetic field applied perpendicular to the flow direction, comparison can be only done for open bored MRI simulations.

Reduction in axial velocity by increasing the magnetic field is due to the fact that as magnetic field applied, the Lorentz force opposes the flow of blood and magnetic particles, which reduces the axial flow velocity.

When the domain is under external magnetic field, velocity contours and WSS are calculated. In concordance with results shown in [154] WSS on the magnetic models differ considerably from the non-magnetic model. It is due to a considerable effect of the external magnetic field on the flow pattern. Taking into account the differences between WSS results from the bottom and top surface of the stent, it is observed that the flow separation takes place on the bottom side of the stent wall. Except for the regions near the proximal and distal necks, WSS value is small in large section of the stent. The variation of WSS on the proximal region of the sent indicated that there is flow separation in that region of the stent wall, this phenomenon also occurs in non-magnetic simulations [162]. After bibliographical review, this is the first time the velocity contours and WSS is compared for a treated aneurysm under eight different magnetic field configurations.

Based on the hypothesis that when the domain is under magnetic field, cells will be attracted and maintained to promote the tissue growing, discrete phase model is performed to study cells motion. As Bose *et al* [154] particle captured simulation, particles are moving due to the blood flow, in this sense changes in the velocity field are relevant. Particles are following the streamlines of blood flow due to the magnetic presence. It is assumed that any droplet released from the same location with the same conditions will follow the same trajectory. In this sense the fluid affects the momentum/energy of the disperse phase, but the surrounding fluid flow (blood) remains unaffected. It is possible to use the DPM as a post–processing exercise, and quickly compute the particle solution. The study by [163] shows the capture efficiency under magnetic fields with different amplitudes. In concordance with their study, from Table 6-5 it is noted that capture

efficiency increases with larger magnetic field strength, indicating a more significant impact of magnetic force on cells motion with larger magnetic field strength. However, according with statistical analysis, the direction of magnetic field has a greater incidence on cells capture efficiency. This findings correspond with results presented by Cherry *et al*, [110] who found that changing magnetic direction significantly improved particle retention. In their study it is shown that it is possible to trap more particles when magnetic field was applied in cross-stream direction vs a magnetic field in streamwise direction. It can be explained from current simulation that as soon as the cells are injected, they are pushed to the ostium and gets trapped by the stent.

In contrast to the previous cases, where practically two-dimensional situation is presented, Kenjeres *et al*, [164] presented a geometry where blood flows inside a 90º bent tube with 4 differently imposed magnetic fields originating from a current wire. The change in the magnetic field direction shows that capturing efficiency increase while more area is exposed to the magnetization force. This simulation allows to realize that there is incidence on the magnetic field direction on the capturing efficiency. However, besides the geometrical differences it is not possible to do a direct comparison between the results since in Kenjeres *et al* model, the magnetic field is not over all the domain, as it is in the present thesis, where the combined effect between treated aneurysm geometry and magnetic configuration is studied.

To classify the factors incidence over the magnetic cells targeting efficacy, postprocessing particle tracking is used to identify the fate of each particle after the injection.
Three possibilities are physically allowed for the particles when they cross the boundaries: escape is used when the particle reach the outlet boundary; trap, when the particle hits the stent wall and reflect when particles hit the vessel wall. Moreover, incomplete fate is presented when particles do not reach none of the above options. It is known that due to the blood flows under external magnetic field effect, particles may naturally become stuck in a recirculation region, and therefore incomplete is appropriate [95].

Magnetic particle motion in the vascular system is governed by magnetic Lorentz force, fluid drag force and Shaffman lift force, particle blood cells interactions, inertia, thermal kinetics and interparticle effects such us magnetic dipole interactions analysis is beyond

the scope of this work. In addition, the present model considers only steady state condition. The transient case may increase the understanding of particle deposition in the stent.

Magnetic configurations simulated correspond to physical possible configurations. The analysis of different options allows to virtually consider the options and the influence of them before proposing a configuration that play a valuable role in clinical decision- making This study represents the first time that a factorial design has been applied to characterize the relationships between external magnetic field features and hemodynamics in wide neck treated saccular brain aneurysm geometry. The numerical models put in evidence the crucial aspects of the flow field from the point of view of the particle accumulation in the targeted region.

7. Neglected effects and results limitations

The purpose of this work is the numerical simulation blood flow pattern of a vascular section, which includes a saccular aneurysm, before and after the interposition of a flow divertor as an endovascular treatment. Computationally, it is sought to simulate an idealized suspension of endothelial cells, labelled with magnetic nanoparticles, and to characterize their behavior under the influence of different external magnetic fields.

In an attempt to simulate realistic conditions, various hemodynamic parameters were investigated by making, for example, geometric changes in idealized models of aneurysms. Also, a realistic magnetic field configurations are used in eight different combination, thus inducing variable flow behavior. Still, several assumptions and simplifications need to be done, which are motivated, by required computational time saving.

An incompressible fluid is assumed, the viscous, non-Newtonian component is implemented, and Non-pulsatile flow condition are applied. Laminar flow is assumed, and the effects of turbulence, recirculation and vortices created in the entrance and exit of the aneurysm sac are not studied.

Although theoretically vessel wall motion has a significant impact on the flow. In this thesis the rugosity in the wall of the blood vessel is considered negligible and it is simulated as rigid. It is acceptable since intracranial arteries do not distend, if it is compared to arteries located outside the cranium.

It is mentioned that different types of cells have been studied as magnetic cell therapy, such as: mesenchymal stem cells, smooth muscle cells, fibroblasts, endothelial progenitor

cells. It is also mentioned that endothelial progenitor cells have the best behavior in the regeneration of vascular tissue. However, in the computational model, instead of having cells labeled with magnetic nanoparticles, selected cells are simplified to particles of 10 um in diameter that only respond to the magnetic charge.

The obtained results are limited to conclude on cellular magnetic attraction, considering that there are other fluid dynamics factors such as current and shear stress, which depend on cell geometry and viscous factors.

With the obtained results it is not possible to guess that the use of living cells generates a recovery of the vessel, by generating cell growth or pseudo neoendothelization. It cannot be affirmed that the regeneration of the tunica media vascular in the neck of the aneurysm in this case would prevent the entry of blood into the aneurysmal sac reducing the pressure that is the cause of the rupture.

The study ignores all histochemical and mechanotransduction activity, which helps growth and endothelization process. In addition, despite a thrombogenic response occurs after platelet deposition and clotting activation, the thrombus formation provided by the medical device is neglected.

8. Conclusions

Taking into account that the long-term effects of magnetic labelled cells flowing in blood flow and whether they facilitate endothelialization in stent wall are still unknown, this work helps to improve the fundamental understanding of the hemodynamics changes in treated aneurysm under magnetic fields. and promotes the hemodynamics-based predictions of treatment outcomes from novel treatment strategies, that could impact patient outcomes.

This work aimed to describe the changes in the endothelial cells flow conditions in an idealized saccular brain aneurysm model, under external magnetic field, as part of a novel treatment to recruit cells to the stent location. Using bibliographical review, the representative geometrical configuration, the boundary conditions and the mechanical properties needed for calculating the disturbed blood flow parameters inside a wide-neck aneurysm in the presence of a uniform magnetic field is proposed.

After studying the changes in blood velocity and WSS related with the magnetic field presence, a suspension of particles to represent idealized endothelial cells, is computationally injected, the trajectory is modeled and the particles that are trapped on the stent spires are quantified. By the time when the bibliographical review was done, there was not similar studies that allow to appraise the combination of magnetic field amplitude, frequency, duration and direction required to attract and maintain particles to a stent. This thesis proposes the study of low and high value for each variable according with realistic conditions, as availability of MRI devices. With this, it is possible to understand the changes in the flow conditions of the particles and to examine whether, when the blood flow is subjected to an external magnetic field, it is possible to trap them in the region of the stent. It is found that when particle suspension is injected to the blood flow in presence of an external magnetic field, particles are successfully captured in the stent region, whereas it is not the case for non-magnetized model.

The virtual stent models have shown an influence in blood flow velocity which in turn modifies the particles motions in the region of interest. To classify the factors incidence over the magnetic cells targeting efficacy a null hypothesis is established. It indicates that if the amplitude, frequency and direction of the magnetic field applied to the region of interest changed, then there is not significant difference in the capture efficiency on the stent region.

With a P value ≤ 0.05 it is indicated strong evidence against the null hypothesis, being rejected. From the DOE analysis, it is possible to conclude that the classification of the factors incidence over the magnetic particle targeting efficacy includes the amplitude of the magnetic field. This conclusion is supported by a number of studies where magnetic field strength has been varied.

Results are considered to be spatially independent of the computational mesh when differences in the WSS were less than 6% between successive mesh densities. It allows to define mesh-independent solutions to achieve an appropriate grid for predicting the behavior of biomagnetic fluid flow in the presence of the magnetic field .

Taking into account the scope of the present thesis, it is concluded that numerical simulations can yield a better understanding of the physical behavior of ECs flow. In this respect, it is essential to correctly define the representative geometrical configuration, the boundary conditions and the mechanical properties needed for calculating the disturbed blood flow parameters inside a wide-neck aneurysm in the presence of a uniform magnetic field are defined. Mesh-independent solutions is also required to achieve an appropriate grid for predicting the behavior of biomagnetic fluid flow in the presence of the magnetic field. In addition, the set up defined for the CFD analysis highly influence the results and the satisfactory level of understanding of the phenomenon in the shortest possible time and reducing the number of in vitro experiments. To sum up, CFD simulation helps to accelerate the pre-clinical test for new IA aneurysm treatments.

Main differences of this study from previous work are the magnetic field configuration incidence analysis on the cells capture efficiency. As a matter of fact, it is the first to variate magnetic field amplitude, frequency and direction in the residence time duration of the particles.

This model is designed for idealized analysis. Eventually, the hemodynamics metrics will be useful for predict treatment outcome improving actual treatment results.

9. Future Work

Understanding the hemodynamics of intracranial aneurysms is essential for predicting the treatment success. The virtual investigation done in this thesis using idealized models, helps to understand the phenomenon in a first stage. However, complete the CFD simulations of blood flow with patient-individual data will reduce the number of assumptions improving the reliability of the results. Patient individual data includes and are not limited to understand the influence of the pulsatile blood condition, patient specific aneurysm geometry reconstructed from medical images and integrate the interaction particle-fluid-structure under the incidence of the magnetic field.

In the pursuit of the optimal magnetic field design to attract and maintain endothelial cells in the stent region. This thesis considered the incidence of the magnetic field amplitude, frequency and direction, factors that are related with the external magnetic field source. To have a better understanding of the phenomenon, other factors related with the phenomenon are suggested to be examined including the effect of magnetizable stents and the interaction among magnetic particles.

Using the methodology presented in this thesis, it is possible to compare various stent designs and to establish their limitations in the capture efficiency under the effect of different magnetic fields. Regarding the capture efficiency, besides knowing the number of particles trapped in a region, it would be interesting for complete endothelialization studies to understand where the particles are located. This approach may lead to better understanding of the magnetic effects to propose more improvements in long-term device performance.

In addition to patient-specific hemodynamic simulations, experimental approach is required to identify differences between the individual velocities as well as stent shear stresses at the stent and to gain more experience with the hemodynamics changes induced by the magnetic field presence.

More simulations are suggested to evaluate further discrete phase boundary condition types around the proposal of the novel treatment to recruit cells to the stent location. In the current model, an ideal stick condition is used, while the spread and splash options are neglected in addition the investigation of agglomeration of particles is not considered.

References

[1] Brain Aneurysm Foundation, “Brain Aneurysm Statistics and Facts – Brain Aneurysm Foundation,” 2018. [Online]. Available: http://www.bafound.org/about-brain-aneurysms/brain-aneurysm-basics/brain-aneurysm-statistics-and-facts/. [Accessed: 04-Sep-2016].

[2] M. Mehra, G. Spilberg, M. J. Gounis, and A. K. Wakhloo, *Biomechanics and Mechanobiology of Aneurysms.*, vol. 7. Heidelberg: Springer Berlin Heidelberg, 2011.

[3] B. J. Doyle and T. McGloughlin, “Towards an Improvement in Aneurysm Assessment: Coupling 3D Reconstruction Tools with Engineering Know-How,” Ireland, 2009.

[4] M. H. Babiker *et al.*, “Influence of stent configuration on cerebral aneurysm fluid dynamics.,” *J. Biomech.*, vol. 45, no. 3, pp. 440–7, Feb. 2012.

[5] B. Daou and P. Jabbour, “Flow Diversion for Treating Middle Cerebral Artery Aneurysms,” *World Neurosurg.*, vol. 90, pp. 627–629, 2016.

[6] O. M. M. Topcuoglu *et al.*, “Flow Diversion in Middle Cerebral Artery Aneurysms: Is It Really an All-Purpose Treatment?,” *World Neurosurg.*, vol. 87, pp. 317–327, Mar. 2016.

[7] Y. Zhang, W. Chong, and Y. Qian, “Investigation of intracranial aneurysm hemodynamics following flow diverter stent treatment.,” *Med. Eng. Phys.*, vol. 35, no. 5, pp. 608–15, May 2013.

[8] I. Chatziprodromou, A. Tricoli, D. Poulikakos, and Y. Ventikos, “Haemodynamics and wall remodelling of a growing cerebral aneurysm: a computational model.,” *J. Biomech.*, vol. 40, no. 2, pp. 412–26, Jan. 2007.

[9] J. P. Allain, T. Tigno, and R. Armonda, *Nanotechnology for Cerebral Aneurysm Treatment*. Babak Kateb and John D. Heiss, 2013.

[10] P. Berg, C. Iosif, S. Ponsonnard, C. Yardin, G. Janiga, and C. Mounayer, “Endothelialization of over- and undersized flow-diverter stents at covered vessel side branches: An in vivo and in silico study,” *J. Biomech.*, vol. 49, no. 1, pp. 4–12, 2016.

[11] J. P. Allain, L. Reece, Z. Yang, R. Armonda, R. Kempaiah, and T. Tigno, “System and stent for repairing endovascular defects and methods of use,” WO2013052934

A3, CA2851264A1, EP2763710A2, EP2763710A4, US20140277354, WO2013052934A2, 30-May-2013.

[12] T. J. Tigno, “Systems and methods for magnetized stent having growth-promoting properties,” CA2803385A1; EP2590600A1; US20130110225; WO2012006373A1; US9283095 B2, 15-Mar-2016.

[13] A. Adibi, A. Sen, and A. P. Mitha, “Cell Therapy for Intracranial Aneurysms: A Review,” *World Neurosurg.*, vol. 86, pp. 390–398, 2016.

[14] S. V. Pislaru *et al.*, “Magnetically Targeted Endothelial Cell Localization in Stented Vessels,” *J. Am. Coll. Cardiol.*, vol. 48, no. 9, pp. 1839–1845, 2006.

[15] J. J. Connell, P. S. Patrick, Y. Yu, M. F. Lythgoe, and T. L. Kalber, “Advanced cell therapies: targeting, tracking and actuation of cells with magnetic particles,” *Regen. Med.*, vol. 10, no. 6, pp. 757–772, Sep. 2015.

[16] B. Polyak *et al.*, “High field gradient targeting of magnetic nanoparticle-loaded endothelial cells to the surfaces of steel stents.,” *Proc. Natl. Acad. Sci. U. S. A.*, vol. 105, no. 2, pp. 698–703, Jan. 2008.

[17] J.-J. Chiu *et al.*, “Analysis of the effect of disturbed flow on monocytic adhesion to endothelial cells,” *J. Biomech.*, vol. 36, no. 12, pp. 1883–1895, 2003.

[18] H. P. Wendel, M. Avci-Adali, and G. Ziemer, “Endothelial progenitor cell capture stents — hype or hope?,” 2010.

[19] M. Avci-Adali, G. Ziemer, and H. P. Wendel, “Induction of EPC homing on biofunctionalized vascular grafts for rapid in vivo self-endothelialization — A review of current strategies,” *Biotechnol. Adv.*, vol. 28, no. 1, pp. 119–129, 2010.

[20] M. A. Ostrowski *et al.*, “Microvascular Endothelial Cells Migrate Upstream and Align Against the Shear Stress Field Created by Impinging Flow,” *Biophys. J.*, vol. 106, no. 2, pp. 366–374, 2014.

[21] E. Carenza *et al.*, “In vitro angiogenic performance and in vivo brain targeting of magnetized endothelial progenitor cells for neurorepair therapies,” *Nanomedicine Nanotechnology, Biol. Med.*, vol. 10, no. 1, pp. 225–234, Jan. 2014.

[22] L. Boldock, “The Influence of Stent Geometry on Haemodynamics and Endothelialisation,” The University of Sheffield, 2017.

[23] D. Kocur *et al.*, “Stent-assisted embolization of wide-neck anterior communicating artery aneurysms: Review of consecutive 34 cases,” *Neurol. Neurochir. Pol.*, 2016.

[24] A. Di Carlos, V. Sansalone, A. Tatone, and V. Varano, “Growth and Remodelling of Intracranial Saccular Aneurysms,” in *COMSOL Conference in Milan*, 2009, pp. 1–7.

[25] A. Selimovic, Y. Ventikos, and P. N. Watton, “Modelling the Evolution of Cerebral Aneurysms: Biomechanics, Mechanobiology and Multiscale Modelling,” *Procedia IUTAM*, vol. 10, pp. 396–409, 2014.

[26] J. P. D. Mark R. Harrigan, *Handbook of cerebrovascular diseases and neurointervetional technique*. 2013.

[27] P. M. Munarriz, P. A. Gómez, I. Paredes, A. M. Castaño-Leon, S. Cepeda, and A. Lagares, “Basic Principles of Hemodynamics and Cerebral Aneurysms,” *World Neurosurg.*, vol. 88, pp. 311–319, 2016.

[28] L. R. Caplan, “Basic Pathology, Anatomy, and Pathophysiology of Stroke,” *Caplan’s Stroke*, pp. 22–63, 2009.

[29] W. Cai, C. Hu, J. Gong, and Q. Lan, “Anterior Communicating Artery Aneurysm Morphology and the Risk of Rupture,” *World Neurosurg.*, vol. 109, pp. 119–126, 2018.

[30] M. A. Castro, C. M. Putman, M. J. Sheridan, and J. R. Cebral, “Hemodynamic Patterns of Anterior Communicating Artery Aneurysms: A Possible Association with Rupture,” *Am. J. Neuroradiol.*, vol. 30, no. 2, 2009.

[31] F. Liang, X. Liu, R. Yamaguchi, and H. Liu, “Sensitivity of flow patterns in aneurysms on the anterior communicating artery to anatomic variations of the cerebral arterial network,” *J. Biomech.*, vol. 49, no. 15, pp. 3731–3740, Nov. 2016.

[32] H.-J. Steiger, N. Etminan, and D. Hänggi, “The Current State of Aneurysm Microsurgery,” in *Microsurgical Brain Aneurysms*, Berlin, Heidelberg: Springer Berlin Heidelberg, 2015, pp. 1–5.

[33] B. J. Doyle and T. McGloughlin, “Towards an Improvement in Aneurysm Assessment: Coupling 3D Reconstruction Tools with Engineering Know-How,” Ireland, 2009.

[34] A. M. Karacozoff, F. G. Shellock, and A. K. Wakhloo, “A next-generation, flow-diverting implant used to treat brain aneurysms: in vitro evaluation of magnetic field interactions, heating and artifacts at 3-T,” *Magn. Reson. Imaging*, vol. 31, no. 1, pp. 145–149, 2013.

[35] M. Mehra, G. Spilberg, M. J. Gounis, and A. K. Wakhloo, “Intracranial Aneurysms: Clinical Assessment and Treatment Options,” 2011, pp. 331–372.

[36] A. M. Karacozoff, F. G. Shellock, and A. K. Wakhloo, “A next-generation, flow-diverting implant used to treat brain aneurysms: in vitro evaluation of magnetic field interactions, heating and artifacts at 3-T,” *Magn. Reson. Imaging*, vol. 31, no. 1, pp. 145–149, 2013.

[37] T. Kikuchi, A. Ishii, H. Chihara, and S. Miyamoto, “Occlusion Status on Magnetic Resonance Angiography Is Associated with Risk of Delayed Ischemic Events in Cerebral Aneurysms Treated with Stent-Assisted Coiling,” *World Neurosurg.*, vol. 107, pp. 226–232, Nov. 2017.

[38] B. Daou and P. Jabbour, “Flow Diversion for Treating Middle Cerebral Artery Aneurysms,” 2016.

[39] G. Lanzino, “Flow diversion for intracranial aneurysms,” *J. Neurosurg.*, vol. 118, no. 2, pp. 405–407, Feb. 2013.

[40] R. Sethi and C. Lee, “Endothelial Progenitor Cell Capture Stent: Safety and Effectiveness,” *J. Interv. Cardiol.*, vol. 25, no. 5, pp. 493–500, Oct. 2012.

[41] R. F. Adamo *et al.*, “Magnetically enhanced cell delivery for accelerating recovery of the endothelium in injured arteries,” *J. Control. Release*, vol. 222, pp. 169–175, 2016.

[42] A. Kumar, R. Jakubovic, V. Yang, and L. Dacosta, “Traumatic anterior cerebral artery aneurysms and management options in the endovascular era,” *J. Clin. Neurosci.*, vol. 25, pp. 90–95, 2016.

[43] K. Larsen *et al.*, “Capture of circulatory endothelial progenitor cells and accelerated re-endothelialization of a bio-engineered stent in human ex vivo shunt and rabbit denudation model,” *Eur. Heart J.*, vol. 33, no. 1, pp. 120–128, Jan. 2012.

[44] J. R. Cebral *et al.*, “Analysis of hemodynamics and aneurysm occlusion after flow-diverting treatment in rabbit models.,” *AJNR. Am. J. Neuroradiol.*, vol. 35, no. 8, pp. 1567–73, Aug. 2014.

[45] A. Fortier, V. Gullapalli, and R. A. Mirshams, “Review of biomechanical studies of arteries and their effect on stent performance,” *IJC Hear. Vessel.*, vol. 4, pp. 12–18, 2014.

[46] A. G. Kutikhin, M. Y. Sinitsky, A. E. Yuzhalin, and E. A. Velikanova, “Shear stress: An essential driver of endothelial progenitor cells,” *J. Mol. Cell. Cardiol.*, vol. 118, pp. 46–69, May 2018.

[47] A. P. Antoniadis *et al.*, “Biomechanical Modeling to Improve Coronary Artery Bifurcation Stenting,” *JACC Cardiovasc. Interv.*, vol. 8, no. 10, pp. 1281–1296, Aug. 2015.

[48] K. Gregory-Evans, A. E. Bashar, and C. Laver, “Use of magnetism to enhance cell transplantation success in regenerative medicine,” *Regen. Med.*, vol. 8, no. 1, pp. 1–3, Jan. 2013.

[49] S. V. Pislaru *et al.*, “Magnetic Forces Enable Rapid Endothelialization of Synthetic Vascular Grafts,” *Circulation*, vol. 114, no. 1_suppl, pp. I-314-I–318, Jul. 2006.

[50] S. L. Arias, A. R. Shetty, A. Senpan, M. Echeverry-Rendón, L. M. Reece, and J. P. Allain, “Fabrication of a Functionalized Magnetic Bacterial Nanocellulose with Iron Oxide Nanoparticles.,” *J. Vis. Exp.*, no. 111, 2016.

[51] R. R. Ravindranath, A. Romaschin, and M. Thompson, “In vitro and in vivo cell-capture strategies using cardiac stent technology — A review,” *Clin. Biochem.*, vol. 49, no. 1, pp. 186–191, 2016.

[52] M. Marosfoi *et al.*, “In situ tissue engineering: endothelial growth patterns as a function of flow diverter design,” *J. Neurointerv. Surg*, vol. 34, no. 1, pp. 16–17,

2016.

[53] J. P. Aronson *et al.*, “A novel tissue engineering approach using an endothelial progenitor cell–seeded biopolymer to treat intracranial saccular aneurysms,” *J. Neurosurg.*, vol. 117, no. 3, pp. 546–554, 2012.

[54] K. Alkhalili *et al.*, “The Effect of Stents in Cerebral Aneurysms : A Review,” vol. 13, no. 2, pp. 201–211, 2018.

[55] L. Campo-Deaño, M. S. N. Oliveira, and F. T. Pinho, “A Review of Computational Hemodynamics in Middle Cerebral Aneurysms and Rheological Models for Blood Flow,” *Appl. Mech. Rev.*, vol. 67, no. 3, p. 030801, 2015.

[56] P. Nair *et al.*, “Hemodynamic characterization of geometric cerebral aneurysm templates,” *J. Biomech.*, vol. 49, no. 11, pp. 2118–2126, 2016.

[57] A. Valencia, H. Morales, R. Rivera, E. Bravo, and M. Galvez, “Blood flow dynamics in patient-specific cerebral aneurysm models: the relationship between wall shear stress and aneurysm area index.,” *Med. Eng. Phys.*, vol. 30, no. 3, pp. 329–40, Apr. 2008.

[58] E. Lopez Ramirez, “Numerical Investigation of Blood Flow in Stented Intracranial Aneurysms Models,” Friedrich-Alexander-Universität Erlangen-Nürnberg (FAU), 2011.

[59] W. Jeong and K. Rhee, “Hemodynamics of cerebral aneurysms: computational analyses of aneurysm progress and treatment.,” *Comput. Math. Methods Med.*, vol. 2012, no. 1748–670X, p. 782801, Jan. 2012.

[60] M. Aenis, A. P. Stancampiano, A. K. Wakhloo, and B. B. Lieber, “Modeling of flow in a straight stented and nonstented side wall aneurysm model.,” *J. Biomech. Eng.*, vol. 119, no. 2, pp. 206–12, May 1997.

[61] M. L. Rossi, D. Zavalloni, and P. Presbitero, “Replay to the article by Wendel HP et al.: Endothelial progenitor cell capture stents — Hype or hope?,” *Int. J. Cardiol.*, vol. 145, no. 1, pp. 117–118, Nov. 2010.

[62] B. D. Plouffe, S. K. Murthy, and L. H. Lewis, “Fundamentals and application of magnetic particles in cell isolation and enrichment: A review,” *Reports Prog. Phys.*, vol. 78, no. 1, 2015.

[63] M. Calero *et al.*, “Efficient and safe internalization of magnetic iron oxide nanoparticles: Two fundamental requirements for biomedical applications,” *Nanomedicine Nanotechnology, Biol. Med.*, vol. 10, no. 4, pp. 733–743, May 2014.

[64] R. S. Molday, S. P. S. Yen, and A. Rembaum, “Application of magnetic microspheres in labelling and separation of cells,” *Nature*, vol. 268, pp. 437–8, 1977.

[65] P. M. Consigny, D. A. Silverberg, and N. J. Vitali, “Use of Endothelial Cells Containing Superparamagnetic Microspheres to Improve Endothelial Cell Delivery

to Arterial Surfaces after Angioplasty," *J. Vasc. Interv. Radiol.*, vol. 10, no. 2, pp. 155–163, Feb. 1999.

[66] J. Dobson, "Remote control of cellular behaviour with magnetic nanoparticles," *Nat. Nanotechnol.*, vol. 3, no. 3, pp. 139–143, 2008.

[67] L. Cheng *et al.*, "Multifunctional upconversion nanoparticles for dual-modal imaging-guided stem cell therapy under remote magnetic control," *Adv. Funct. Mater.*, vol. 23, no. 3, pp. 272–280, 2013.

[68] E. Duguet, S. Vasseur, S. Mornet, and J. M. Devoisselle, "Magnetic nano-particles and their applications in medicine," *Futur. Med.*, vol. 48, no. 5, pp. 999–1003, 2006.

[69] J. Kolosnjaj-Tabi, C. Wilhelm, O. Clément, and F. Gazeau, "Cell labeling with magnetic nanoparticles: opportunity for magnetic cell imaging and cell manipulation.," *J. Nanobiotechnology*, vol. 11 Suppl 1, no. Suppl 1, pp. 1–19, 2013.

[70] H. Shen, S. Tong, G. Bao, and B. Wang, "Structural responses of cells to intracellular magnetic force induced by superparamagnetic iron oxide nanoparticles.," *Phys. Chem. Chem. Phys.*, vol. 16, no. 5, pp. 1914–20, 2014.

[71] H. Koiwaya *et al.*, "Augmented neovascularization with magnetized endothelial progenitor cells in rats with hind-limb ischemia," *J. Mol. Cell. Cardiol.*, vol. 51, no. 1, pp. 33–40, Jul. 2011.

[72] R. Sensenig, Y. Sapir, C. MacDonald, S. Cohen, and B. Polyak, "Magnetic nanoparticle-based approaches to locally target therapy and enhance tissue regeneration in vivo.," *Nanomedicine (Lond).*, vol. 7, no. 9, pp. 1425–42, Sep. 2012.

[73] A. G. J. Tibbe, B. G. De Grooth, J. Greve, G. J. Dolan, C. Rao, and L. W. M. M. Terstappen, "Magnetic field design for selecting and aligning immunomagnetic labeled cells," *Cytometry*, vol. 47, no. 3, pp. 163–172, 2002.

[74] S. Uthamaraj, B. J. Tefft, O. Hlinomaz, G. S. Sandhu, and D. Dragomir-Daescu, "Ferromagnetic Bare Metal Stent for Endothelial Cell Capture and Retention.," *J. Vis. Exp.*, no. 103, Sep. 2015.

[75] Y. Shen *et al.*, "Comparison of magnetic intensities for mesenchymal stem cell targeting therapy on ischemic myocardial repair: High magnetic intensity improves cell retention but has no additional functional benefit," *Cell Transplant.*, vol. 24, no. 10, pp. 1981–1997, 2015.

[76] S. Rashidi, J. A. Esfahani, and M. Maskaniyan, "Applications of magnetohydrodynamics in biological systems-a review on the numerical studies," *J. Magn. Magn. Mater.*, vol. 439, pp. 358–372, 2017.

[77] T. Lunnoo and T. Puangmali, "Capture Efficiency of Biocompatible Magnetic Nanoparticles in Arterial Flow: A Computer Simulation for Magnetic Drug Targeting," *Nanoscale Res. Lett.*, vol. 10, no. 1, 2015.

[78] S. Bose and M. Banerjee, “Effect of non-Newtonian characteristics of blood on magnetic particle capture in occluded blood vessel,” *J. Magn. Magn. Mater.*, vol. 374, pp. 611–623, 2015.

[79] O. Pourmehran, M. Rahimi-Gorji, M. Gorji-Bandpy, and T. B. Gorji, “Simulation of magnetic drug targeting through tracheobronchial airways in the presence of an external non-uniform magnetic field using Lagrangian magnetic particle tracking,” *J. Magn. Magn. Mater.*, vol. 393, pp. 380–393, 2015.

[80] S. Sharma, V. K. Katiyar, and U. Singh, “Mathematical modelling for trajectories of magnetic nanoparticles in a blood vessel under magnetic field,” *J. Magn. Magn. Mater.*, vol. 379, pp. 102–107, 2015.

[81] S. Majee and G. C. Shit, “Numerical investigation of MHD flow of blood and heat transfer in a stenosed arterial segment,” *J. Magn. Magn. Mater.*, vol. 424, pp. 137–147, 2017.

[82] J. Overweg, “MRI main field magnets,” *Phys*, vol. 38, pp. 25–63, 2008.

[83] T. C. Cosmus and M. Parizh, “Advances in Whole-Body MRI Magnets,” vol. 2109, no. 14, pp. 2104–2109, 2011.

[84] S. M. Blinder, “Quantum Chemistry,” no. 3. Michigan, pp. 1–12, 2002.

[85] A. Nacev, C. Beni, O. Bruno, and B. Shapiro, “The behaviors of ferromagnetic nano-particles in and around blood vessels under applied magnetic fields,” *J. Magn. Magn. Mater.*, vol. 323, no. 6, pp. 651–668, 2011.

[86] S. N. Mirzababaei, T. B. Gorji, M. Baou, M. Gorji-Bandpy, and N. Fatouraee, “Investigation of magnetic nanoparticle targeting in a simplified model of small vessel aneurysm,” *J. Magn. Magn. Mater.*, vol. 426, pp. 126–131, Mar. 2017.

[87] S. Sharma, U. Singh, and V. K. Katiyar, “Magnetic field effect on flow parameters of blood along with magnetic particles in a cylindrical tube,” *J. Magn. Magn. Mater.*, vol. 377, pp. 395–401, 2015.

[88] S. Kayal *et al.*, “The flow of magnetic nanoparticles in magnetic drug targeting,” *RSC Adv.*, vol. 1, no. 2, p. 238, 2011.

[89] A. Hajiaghajani, S. Hashemi, and A. Abdolali, “Adaptable setups for magnetic drug targeting in human muscular arteries: Design and implementation,” *J. Magn. Magn. Mater.*, vol. 438, pp. 173–180, Sep. 2017.

[90] P. S. Patrick, Q. A. Pankhurst, C. Payne, T. L. Kalber, and M. F. Lythgoe, “Magnet-Targeted Delivery and Imaging,” in *Design and Applications of Nanoparticles in Biomedical Imaging*, Cham: Springer International Publishing, 2017, pp. 123–152.

[91] C. . Taylor and J. D. Humphrey, “Open problems in computational vascular biomechanics: Hemodynamics and arterial wall mechanics,” *Comput. Methods Appl. Mech. Eng.*, vol. 198, no. 45–46, pp. 3514–3523, Sep. 2009.

[92] P. Berg, D. Stucht, G. Janiga, O. Beuing, O. Speck, and D. Thévenin, “Cerebral Blood Flow in a Healthy Circle of Willis and Two Intracranial Aneurysms: Computational Fluid Dynamics Versus Four-Dimensional Phase-Contrast Magnetic Resonance Imaging,” *J. Biomech. Eng.*, vol. 136, no. 4, p. 041003, Mar. 2014.

[93] L. Duque-Ortega, S. Correa Vélez, and C. M. Jiménez Yepez, “Computational fluid dynamics in intracranial aneurysm,” *CES Med.*, vol. 29, no. 2, pp. 239–254, 2015.

[94] A. D. Caballero and S. Laín, “A Review on Computational Fluid Dynamics Modelling in Human Thoracic Aorta,” *Cardiovasc. Eng. Technol.*, vol. 4, no. 2, pp. 103–130, 2013.

[95] S. I. Bernad, A. F. Totorean, and L. Vekas, “Particles deposition induced by the magnetic field in the coronary bypass graft model,” *J. Magn. Magn. Mater.*, vol. 401, pp. 269–286, 2016.

[96] H. Aminfar, M. Mohammadpourfard, and K. Khajeh, “Mechanobiology of LDL mass transport in the arterial wall under the effect of magnetic field, part I: Diffusion rate,” *J. Magn. Magn. Mater.*, vol. 426, pp. 569–574, 2017.

[97] E. E. Tzirtzilakis, “A mathematical model for blood flow in magnetic field,” *Phys. Fluids*, vol. 17, no. 7, pp. 1–15, 2005.

[98] Y. Haik, V. M. Pai, and C. J. Chen, “Bio-Magnetic Fluid Dynamics,” *Fluid Dyn. Interfaces*, no. January 2013, 1996.

[99] E. J. Furlani and E. P. Furlani, “A model for predicting magnetic targeting of multifunctional particles in the microvasculature,” *J. Magn. Magn. Mater.*, vol. 312, no. 1, pp. 187–193, 2007.

[100] L. Könözsy, P. Scienza, and D. Drikakis, “Validation of a Magneto- and Ferro-Hydrodynamic Model for Non-Isothermal Flows in Conjunction With Newtonian and Non-Newtonian Fluids,” *ECCOMAS Congr. 2016*, no. June, pp. 5–10, 2016.

[101] P. Scienza, “Numerical Investigation of non-Newtonian Biomagnetic Fluid Flows in presence of localized Magnetic Field,” Politecnico di Milano, 2015.

[102] E. E. Tzirtzilakis and V. C. Loukopoulos, “Biofluid flow in a channel under the action of a uniform localized magnetic field,” *Comput. Mech.*, vol. 36(5), pp. 360–374, 2005.

[103] H. Alimohamadi, M. Imani, and M. Shojaeizadeh, “Computational analysis of pulsatile biofluid in a locally expanded vessel under the action of magnetic field,” *Adv. Appl. Sci. Res.*, vol. 4, no. 6, pp. 96–103, 2013.

[104] S. Wang, H. Liu, and W. Xu, “Hydrodynamic modelling and CFD simulation of ferrofluids flow in magnetic targeting drug delivery,” *Int. J. Comut. Fluid Dyn.*, vol. 22, no. 10, pp. 659–667, 2008.

[105] V. L. Rayz *et al.*, “Flow Residence Time and Regions of Intraluminal Thrombus Deposition in Intracranial Aneurysms,” *Ann. Biomed. Eng.*, vol. 38, no. 10, pp.

3058–3069, Oct. 2010.

[106] J. W. Haverkort, S. Kenjereš, and C. R. Kleijn, “Computational simulations of magnetic particle capture in arterial flows,” *Ann. Biomed. Eng.*, vol. 37, no. 12, pp. 2436–2448, 2009.

[107] S. A. Khashan, A. Alazzam, and E. P. Furlani, “Computational analysis of enhanced magnetic bioseparation in microfluidic systems with flow-invasive magnetic elements.,” *Sci. Rep.*, vol. 4, p. 5299, Jun. 2014.

[108] D. C. Cohen Stuart, C. R. Kleijn, and S. Kenjereš, “An efficient and robust method for Lagrangian magnetic particle tracking in fluid flow simulations on unstructured grids,” *Comput. Fluids*, vol. 40, no. 1, pp. 188–194, Jan. 2011.

[109] S. A. Khashan, A. Alazzam, and B. Mathew, “Modeling and simulation of the multiphase flow involving magnetophoresis-based microfluidic systems,” *Proc. SPIE*, vol. 9517, no. June, 2015.

[110] E. M. Cherry and J. K. Eaton, “A comprehensive model of magnetic particle motion during magnetic drug targeting,” *Int. J. Multiph. Flow*, vol. 59, pp. 173–185, Feb. 2014.

[111] M. Reza Habibi and M. Ghasemi, “Numerical study of magnetic nanoparticles concentration in biofluid (blood) under influence of high gradient magnetic field,” *J. Magn. Magn. Mater.*, vol. 323, no. 1, pp. 32–38, 2011.

[112] L. DUQUE-ORTEGA, S. CORREA-VÉLEZ, and C. M. JIMÉNEZ-YEPES, “Computational fluid dynamics in intracranial aneurysm,” *CES Med.*, vol. 29, no. 2, pp. 239–254, 2015.

[113] A. Lozovskiya, M. A.Olshanskiib, V. and Salamatovac, and Y. V.Vassilevskic, “An unconditionally stable semi-implicit FSI finite element method,” *Comput. Methods Appl. Mech. Eng.*, vol. 297, pp. 437–454, Dec. 2015.

[114] S. Voß *et al.*, “Fluid-Structure Simulations of a Ruptured Intracranial Aneurysm: Constant versus Patient-Specific Wall Thickness.,” *Comput. Math. Methods Med.*, vol. 2016, p. 9854539, 2016.

[115] a Valencia and F. Solis, “Blood flow dynamics and arterial wall interaction in a saccular aneurysm model of the basilar artery,” *Comput. Struct.*, vol. 84, pp. 1326–1337, 2006.

[116] R. Torii, M. Oshima, T. Kobayashi, K. Takagi, and T. E. Tezduyar, “Influence of wall thickness on fluid-structure interaction computations of cerebral aneurysms,” *Int. j. numer. method. biomed. eng.*, vol. 26, no. 3–4, pp. 336–347, Mar. 2010.

[117] C. J. Lee, Y. Zhang, H. Takao, Y. Murayama, and Y. Qian, “The influence of elastic upstream artery length on fluid-structure interaction modeling: A comparative study using patient-specific cerebral aneurysm,” *Med. Eng. Phys.*, vol. 35, no. 9, pp. 1377–1384, 2013.

[118] P. Bouillot *et al.*, “Computational fluid dynamics with stents: quantitative comparison with particle image velocimetry for three commercial off the shelf intracranial stents.,” *J. Neurointerv. Surg.*, vol. 8, no. 3, pp. 309–15, Mar. 2016.

[119] A. Qiao and Y. Liu, “Hemodynamics simulation of partly stented aortic arch aneurysm,” *2007 1st Int. Conf. Bioinforma. Biomed. Eng. ICBBE*, no. 3062003, pp. 460–463, 2007.

[120] M. Yahya, “Three dimensional finite-element modeling of blood flow in elastic vessels : effects of arterial geometry and elasticity on aneurysm growth and rupture VESSELS : EFFECTS OF ARTERIAL,” *Диссер*, 2010.

[121] A. Y. Tang and N. Amin, “Some Numerical Approaches to Solve Fluid Structure Interaction Problems in Blood Flow,” *Abstr. Appl. Anal.*, vol. 2014, pp. 1–8, Feb. 2014.

[122] B. Chung and J. R. Cebral, “CFD for Evaluation and Treatment Planning of Aneurysms: Review of Proposed Clinical Uses and Their Challenges,” *Ann. Biomed. Eng.*, vol. 43, no. 1, pp. 122–138, Jan. 2015.

[123] M. Haghdel, R. Kamali, A. Haghdel, and Z. Mansoori, “Effects of non-newtonian properties of blood flow on magnetic nanoparticle targeted drug delivery,” vol. 4, no. 2, pp. 89–97, 2017.

[124] A. Shamloo, M. A. and Nejad, and M. Saeedi, “Fluid–structure interaction simulation of a cerebral aneurysm: Effects of endovascular coiling treatment and aneurysm wall thickening,” *J. Mech. Behav. Biomed. Mater.*, vol. 74, pp. 72–83, Oct. 2017.

[125] A. Alshare and B. Tashtoush, “Simulations of Magnetohemodynamics in Stenosed Arteries in Diabetic or Anemic Models,” vol. 2016, 2016.

[126] M. A. Ikbal, S. Chakravarty, K. K. L. Wong, J. Mazumdar, and P. K. Mandal, “Unsteady response of non-Newtonian blood flow through a stenosed artery in magnetic field,” *J. Comput. Appl. Math.*, vol. 230, no. 1, pp. 243–259, 2009.

[127] S. Kenjereš, “Numerical analysis of blood flow in realistic arteries subjected to strong non-uniform magnetic fields,” *Int. J. Heat Fluid Flow*, vol. 29, no. 3, pp. 752–764, 2008.

[128] R. J. Damiano, D. Ma, J. Xiang, A. H. Siddiqui, K. V Snyder, and H. Meng, “Finite element modeling of endovascular coiling and flow diversion enables hemodynamic prediction of complex treatment strategies for intracranial aneurysm.,” *J. Biomech.*, Jun. 2015.

[129] J. Xu *et al.*, “Combined Effects of Flow Diverting Strategies and Parent Artery Curvature on Aneurysmal Hemodynamics: A CFD Study,” *PLoS One*, vol. 10, no. 9, p. e0138648, Sep. 2015.

[130] P. Tricerri, L. Dedè, S. Deparis, A. Quarteroni, A. M. Robertson, and A. Sequeira,

"Fluid-structure interaction simulations of cerebral arteries modeled by isotropic and anisotropic constitutive laws," *Comput. Mech.*, vol. 55, no. 3, pp. 479–498, Mar. 2015.

[131] D. J. MacDonald, H. M. Finlay, and P. B. Canham, "Directional wall strength in saccular brain aneurysms from polarized light microscopy.," *Ann. Biomed. Eng.*, vol. 28, no. 5, pp. 533–42, May 2000.

[132] P. N. Watton *et al.*, "Modelling Cerebral Aneurysm Evolution," *Stud Mechanobiol Tissue Eng Biomater*, vol. 7, pp. 373–399, 2011.

[133] M. A. Zulliger, P. Fridez, K. Hayashi, and N. Stergiopulos, "A strain energy function for arteries accounting for wall composition and structure," *J. Biomech.*, vol. 37, no. 7, pp. 989–1000, 2004.

[134] V. Costalat *et al.*, "Biomechanical wall properties of human intracranial aneurysms resected following surgical clipping (IRRAs Project)," *J. Biomech.*, vol. 44, no. 15, pp. 2685–2691, 2011.

[135] D. Aranda-Iglesias, C. Ramón-Lozano, and J. A. Rodríguez-Martínez, "Nonlinear resonances of an idealized saccular aneurysm," *Int. J. Eng. Sci.*, vol. 121, no. 0020–7225, pp. 154–166, 2017.

[136] N. Kumar and V. V. Rao, "Hyperelastic Mooney-Rivlin Model : Determination and Physical Interpretation of Material Constants," *MIT Int. J. Mech. Eng.*, vol. 6, no. 1, pp. 43–46, 2016.

[137] T. Richter, *Fluid-structure Interactions: Models, Analysis and Finite Elements*, 118th ed., vol. 118. Magdeburg: Lecture Notes in Computational Science and Engineering, 2017.

[138] S. Ii, K. Sugiyama, S. Takagi, and Y. Matsumoto, "A Computational Blood Flow Analysis in a Capillary Vessel including Multiple Red Blood Cells and Platelets *," *J. Biomech. Sci. Eng.*, vol. 7, no. 1, 2012.

[139] V. M. Pereira *et al.*, "Evaluation of the influence of inlet boundary conditions on computational fluid dynamics for intracranial aneurysms: A virtual experiment," *J. Biomech.*, vol. 46, no. 9, pp. 1531–1539, 2013.

[140] V. Chabannes, M. Ismail, C. Prud'homme, and M. Szopos, "Hemodynamic simulations in the cerebral venous network: A study on the influence of different modeling assumptions," *J. Coupled Syst. Multiscale Dyn.*, vol. 3, no. 1, pp. 23–37, 2015.

[141] T. Guerra, C. Catarino, T. Mestre, S. Santos, J. Tiago, and A. Sequeira, "A data assimilation approach for non-Newtonian blood flow simulations in 3D geometries," vol. 321, pp. 176–194, 2018.

[142] M. K. Banerjee, R. Ganguly, and A. Datta, "Effect of Pulsatile Flow Waveform and Womersley Number on the Flow in Stenosed Arterial Geometry," *ISRN Biomath.*, vol. 2012, pp. 1–17, Nov. 2012.

[143] M. Razzaq, S. Turek, J. Hron, M. Mádlík, H. Wobker, and J. F. Acker, “Numerical simulation of fluid-structure interaction with application to aneurysm hemodynamics,” in *Fluid Structure Interaction II*, Berlin, Heidelberg: Springer, Berlin, Heidelberg, 2009, pp. 193–220.

[144] H. K. Versteeg and W. Malalasekera, *Introduction to Computational Fluid Dynamics*, vol. 44. 2005.

[145] A. Rahbari, M. Fakour, A. Hamzehnezhad, M. A. Vakilabadi, and D. D. Ganji, “Heat transfer and fluid flow of blood with nanoparticles through porous vessels in a magnetic field: A quasi-one dimensional analytical approach,” *Math. Biosci.*, vol. 283, pp. 38–47, 2017.

[146] ANSYS Inc., “ANSYS Fluent Magnetohydrodynamics (MHD) Module Manual,” *ANSYS, Inc.*, 2013. [Online]. Available: http://www.afs.enea.it/project/neptunius/docs/fluent/html/mhd/node11.htm#sec-magnetic-induction. [Accessed: 24-Feb-2018].

[147] Dassault Systemes, “SOLIDWORKS® CAD.” 2016.

[148] ANSYS Inc, “ANSYS® Academic Research Mechanical.” ANSYS, Inc. Private communications, 2018.

[149] Ansys, “ANSYS FLUENT.” 2016.

[150] D. Songsaeng, S. Geibprasert, K. G. ter Brugge, R. Willinsky, M. Tymianski, and T. Krings, “Impact of individual intracranial arterial aneurysm morphology on initial obliteration and recurrence rates of endovascular treatments: a multivariate analysis,” *J. Neurosurg.*, vol. 114, no. 4, pp. 994–1002, 2011.

[151] H. Alimohamadi and M. Imani, “Transient non-newtonian blood flow under magnetic targeting drug delivery in an aneurysm blood vessel with porous walls,” *Int. J. Comput. Methods Eng. Sci. Mech.*, vol. 15, no. 6, pp. 522–533, 2014.

[152] M. Zhao, S. Amin-Hanjani, S. Ruland, A. P. Curcio, L. Ostergren, and F. T. Charbel, “Regional Cerebral Blood Flow Using Quantitative MR Angiography,” *Am. J. Neuroradiol.*, vol. 28, no. 8, pp. 1470–1473, Sep. 2007.

[153] L. Zarrinkoob, K. Ambarki, A. Wåhlin, R. Birgander, A. Eklund, and J. Malm, “Blood flow distribution in cerebral arteries,” *J. Cereb. Blood Flow Metab.*, vol. 35, no. August 2014, pp. 648–654, 2015.

[154] S. Bose and M. Banerjee, “Magnetic particle capture for biomagnetic fluid flow in stenosed aortic bifurcation considering particle-fluid coupling,” *J. Magn. Magn. Mater.*, vol. 385, pp. 32–46, 2015.

[155] R. Zakerzadeh, “A Computational Model for Fluid-Porous Structure Interaction,” *Biomed. Eng. M.Sc. Biomed. Eng.*, 2009.

[156] J.-J. Chiu and S. Chien, “Effects of Disturbed Flow on Vascular Endothelium: Pathophysiological Basis and Clinical Perspectives,” *Physiol. Rev.*, vol. 91, no. 1,

2011.

[157] N. Benard, D. Coisne, E. Donal, and R. Perrault, “Experimental study of laminar blood flow through an artery treated by a stent implantation: characterisation of intra-stent wall shear stress,” *J. Biomech.*, vol. 36, no. 7, pp. 991–998, Jul. 2003.

[158] A. Ghosh, “Targeting Delivery of Magnetic Aerosol Particles To Specific Regions in the Lung,” Queensland University of Technology, 2018.

[159] Minitab, “Minitab.” Pennsylvania, 2018.

[160] F. Ali, A. Imtiaz, I. Khan, and N. A. Sheikh, “Flow of magnetic particles in blood with isothermal heating: A fractional model for two-phase flow,” *J. Magn. Magn. Mater.*, vol. 456, pp. 413–422, 2018.

[161] M. Barbour, “Computational and Experimental Investigation into the Hemodynamics of Endovascularly Treated Cerebral Aneurysms,” University of Washington, 2018.

[162] C. Huang, Z. Chai, and B. Shi, “Non - Newtonian Effect on Hemodynamic Characteristics of Blood Flow in Stented Cerebral Aneurysm,” *Commun . Comput . Phys*, vol. 13, no. 3, pp. 916–928, 2013.

[163] S. Wang, Y. Zhou, J. Tan, J. Xu, J. Yang, and Y. Liu, “Computational modeling of magnetic nanoparticle targeting to stent surface under high gradient field,” *Comput. Mech.*, vol. 53, no. 3, pp. 403–412, 2014.

[164] S. Kenjeres and D. C. Cohen Stuart, “Computational Simulations of Magnetic Particle Capture in Simplified and Realistic Arterial Flows: Towards Optimized Magnetic Drug Targeting,” *Springer, Berlin, Heidelb.*, no. 5, pp. 1006–1009, 2010.